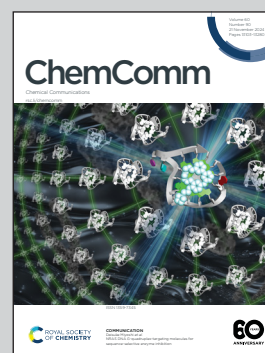Showcasing research from Professor Shudipto K. Dishari and team, Department of Chemical and Biomolecular Engineering, University of Nebraska-Lincoln, Nebraska, United States.

Unravel-engineer-design: a three-pronged approach to advance ionomer performance at interfaces in proton exchange membrane fuel cells

This feature article highlights our efforts to boost the performance of proton exchange membrane fuel cells (PEMFCs) by deepening our understanding of proton conduction in sub-micron thick ionomer films, interface engineering, and creating novel, sustainable and nature-inspired ionomers to enhance proton conduction in thin films.

As featured in:

See Shudipto Konika Dishari *et al.*, *Chem. Commun.*, 2024, **60**, 13114.

ROYAL SOCIETY OF CHEMISTRY

rsc.li/chemcomm

ChemComm

ROYAL SOCIETY
OF CHEMISTRY

FEATURE ARTICLE

Check for updates

Unravel-engineer-design: a three-pronged approach to advance ionomer performance at interfaces in proton exchange membrane fuel cells

Oghenetega Allen Obewhere, [ID] Karen Acurio-Cerda, Sourav Sutradhar, [ID] Moses Dike, Rajesh Keloth [ID] and Shudipto Konika Dishari [ID] *

Proton exchange membrane fuel cells (PEMFCs), which use hydrogen as fuel, present an eco-friendly alternative to internal combustion engines (ICEs) for powering low-to-heavy-duty vehicles and various devices. Despite their promise, PEMFCs must meet strict cost, performance, and durability standards to reach their full potential. A key challenge lies in optimizing the electrode, where a thin ionomer layer is responsible for proton conduction and binding catalyst particles to the electrode. Enhancing ion transport within these sub-µm thick films is critical to improving the oxygen reduction reaction (ORR) at the cathodes of PEMFCs. For the past 15 years, our research has targeted this limitation through a comprehensive "Unravel – Engineer – Design" approach. We first unraveled the behavior of ionomers, gaining deeper insights into both the average and distributed proton conduction properties within sub-µm thick films and at interfaces that mimic catalyst binder layers. Next, we engineered ionomer–substrate interfaces to gain control over interfacial makeup and boost proton conductivity, essential for PEMFC efficiency. Finally, we designed novel nature-derived or nature-inspired, fluorine-free ionomers to tackle the ion transport limitations seen in state-of-the-art ionomers under thin-film confinement. Some of these ionomers even pave the way to address cost and sustainability challenges in PEMFC materials. This feature article highlights our contributions and their importance in advancing PEMFCs and other sustainable energy conversion and storage technologies.

Introduction

Proton exchange membrane fuel cells (PEMFCs) offer an eco-friendly approach to power both low- and high-duty electric vehicles and a range of portable and stationary devices using

Department of Chemical and Biomolecular Engineering, University of Nebraska-Lincoln, Nebraska, USA. E-mail: sdishari2@unl.edu

Oghenetega Allen Obewhere received his BS degree in Biochemistry from the University of Port Harcourt (Nigeria), and MS degree in Materials for Sustainable Energetics from Tallinn University of Technology (Estonia). Currently, he is a PhD candidate in Chemical and Biomolecular Engineering at the University of Nebraska-Lincoln (USA). His research focuses on engineering the ionomer–catalyst interfaces to improve proton con-

Oghenetega Allen Obewhere

ductivity in electrochemical conversion devices.

Karen Acurio-Cerda received her BS degree in Chemical Engineering from Escuela Politécnica Nacional (Ecuador) and MS degree in Environmental and Energy Engineering from the University of Sheffield (UK). She is currently a PhD student in Chemical and Biomolecular Engineering at the University of Nebraska-Lincoln (USA). Her research focuses on the valorization of lignin for biomedical and energy applications.

Karen Acurio-Cerda

H_2, a fuel 3 times more energy dense than gasoline. Unlike traditional internal combustion engines, PEMFCs do not generate greenhouse gases while producing electricity. While PEMFCs have the potential to contribute to a diversified, sustainable and resilient clean energy landscape, to realize their full potential, they must hit the stringent cost-performance-durability targets set by the U.S. Department of Energy (DOE) (Table 1).[1–3]

The membrane electrode assembly (MEA) is the core of many electrochemical conversion and storage systems, including fuel cells. Fuel cells use ion-conducting polymers or ionomers in two formats. In a proton exchange membrane fuel cell (PEMFC), a proton-conducting ionomer membrane, typically several tens of microns thick, separates the anode from the cathode and enables selective proton transport from anode to cathode. The electrodes with ionomer–catalyst layers, on the other hand, serve as the sites for electrochemical reactions within PEMFCs (Fig. 1a). At the PEMFC cathode, a sub-µm thick layer of ionomer glues the catalyst particles to porous carbon electrodes (Fig. 1b and c).[13] This ionomer layer is essential not only for binding catalyst particles to electrodes but also for conducting protons and oxygen to the catalyst interface at the cathode to facilitate the oxygen reduction reaction (ORR, O_2 + $4H^+$ + $4e^-$ → $2H_2O$). While proton transport across the bulk membrane is mostly satisfactory, proton and gas transport within the sub-µm thick ionomer layer over the catalyst

Sourav Sutradhar obtained his BS degree from Shahjalal University of Science and Technology (Bangladesh), and he is currently a PhD student in Chemical & Biomolecular Engineering at the University of Nebraska–Lincoln (USA). His research focuses on optical methods to understand polymers in clean energy systems.

Sourav Sutradhar

Moses Dike obtained his BS degree in Industrial Chemistry from the University of Abuja (Nigeria), and his MS degree in Petroleum Chemistry and Refining from Siberian Federal University (Russia). He is currently a PhD student in Chemical and Biomolecular Engineering at the University of Nebraska-Lincoln (USA). His research focuses on nanoscale electrochemical characterization of ionomers under confinement.

Moses Dike

Rajesh Keloth received his BS degree in Polymer Science and Technology from the Indian Institute of Technology Roorkee (India), followed by his MS degree in Rubber Technology from the Indian Institute of Technology Kharagpur (India). Currently, he is a PhD student in Chemical and Biomolecular Engineering at the University of Nebraska-Lincoln (USA). His research focuses on the modification and characterization of novel synthetic and bio-derived materials for advanced energy applications, including high-temperature proton exchange membrane fuel cells.

Rajesh Keloth

Shudipto Konika Dishari is a Ross McCollum Associate Professor in the Department of Chemical and Biomolecular Engineering at the University of Nebraska-Lincoln (USA). Dishari was a post-doctoral fellow in Chemical Engineering and Materials Science and Engineering at Pennsylvania State University. She received her PhD from National University of Singapore, and BS from Bangladesh University of Engineering and Technology. Dishari's research interests focus on designing synthetic, bio-derived and nature-inspired polymers and nanomaterials for sustainable energy and biomedical technologies. Dishari has received several honors/awards, including, the DOE Office of Science Early CAREER Award, NSF CAREER Award, 3M Non-Tenured Faculty Award, American Chemical Society Polymeric Materials Science and Engineering (ACS PMSE) Young Investigator Award, WEPAN Accelerator Core Concept Award, NUTech Venture Emerging Innovator of the Year Award, and Baxter Young Investigator Award.

Shudipto Konika Dishari

Table 1 Cost-performance-durability targets for PEMFCs

PEMFC performance criteria	LDV/HDV[a]	Current (2023–2024)	Target (year)
Fuel cell system cost ($ per KW)	LDV[b]	64[4]	40 (2030); 30 (2050)[2,5]
	HDV[c]	170[5]	80 (2030); 60 (2050)[2,5]
PGM catalyst loading (mg cm^{-2})[d]	—	>0.4[3]	≤0.3 (2030); ≤0.25 (2050)[3]
Current density at 0.7 V (mA cm^{-2})	—	0.1–1.7[6–8]	3–4 (2030)[9]
Power density (W cm^{-2})	—	1.39[10]	1.8 (2025);[10,11] >2 (2030)[9,10]
Peak efficiency (%)	LDV	64[12]	65 (2030); 70 (2050)[2,5]
	HDV	64[5]	68 (2030); 72 (2050)[2,5]
System lifetime or durability (h)	LDV		5000 (2030), 8000 (2050)[2,5]
	HDV	>10 000[5]	25 000 (2030), 30 000 (2050)[2,5]

[a] LDV: low-duty vehicles, HDV: heavy-duty vehicles. [b] Numbers reported for 80-kW LDV fuel cell systems. [c] Numbers reported for 275-kW HDV fuel cell systems. [d] PGM catalyst: platinum-group metal catalyst.
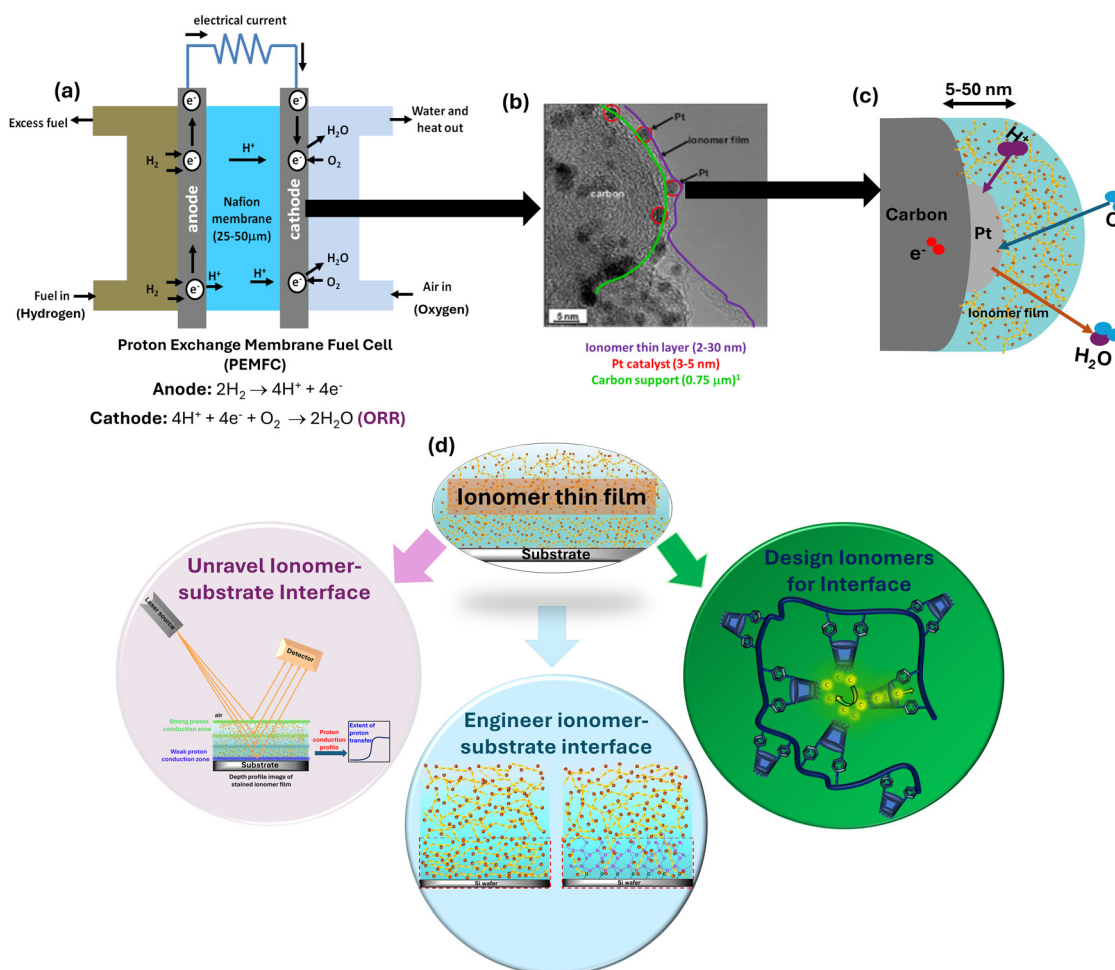

Fig. 1 (a) Schematic showing the basic working principle of a proton exchange membrane fuel cell (PEMFC). (b) High-resolution transmission electron microscopy (TEM) image of the PEMFC catalyst layer[13] showing ionomer–catalyst interface. Corresponding dimensions of carbon support, Pt nanoparticles and ionomer-based thin catalyst binder layer are shown below the TEM image. (c) Schematic view into the cathode catalyst layer depicting the electrochemical oxygen reduction reaction (ORR) at the cathode catalyst layer. (d) Our 3-pronged "Unravel-Engineer-Design" approach to investigate and improve ionomer thin layers on substrate mimicking catalyst binder layer of PEMFC cathode. The TEM image (b) was adapted from ref. 13 with permission from IOP Publishing Ltd. Copyright 2006 The Electrochemical Society.

particles is weak, challenges well known as "ion transport limitation" and "gas transport limitation." As the thin ionomer binder layer conducts protons poorly to the catalyst interfaces, ORR at the cathode slows down, negatively impacting the power generation and overall PEMFC efficiency.[14–22] Historically, research has focused on improving thick bulk ionomer membranes, but the behavior of thin ionomer films has largely been overlooked. Early stage studies suggest that proton conduction

within these sub-μm thick ionomer layer at the catalyst or substrate interface differs significantly from those in bulk membrane separators.[14,16,17,23–25] However, our understanding of the routes to the proton conduction resistance across these thin ionomer layers at interfaces is still at a rudimentary stage and needs a great deal of effort.

To enhance ORR efficiency, first, an in-depth understanding of the morphological, mechanical, and ion-conduction behaviors of ionomers within sub-μm thick films and ionomer–catalyst/ionomer–substrate interfaces is critically needed. A sound, fundamental understanding of ionomer thin films and underlying interfacial phenomena can then inform and guide the engineering-based optimization of the ionomer–catalyst interfaces and new designs of ionomers aimed for catalyst layers/electrodes.

On the interfacial engineering and new ionomer design end, we need to address specific issues associated with ionomer thin films that are already identified and/or we identified through our efforts. To improve the performance at the ionomer–catalyst interfaces, by far much attention has been given to the synthesis of new catalysts,[10,26–28] whereas a feasible and effective route to improve the thin-film proton conductivity could be engineering of the ionomer/catalyst interfaces,[29–32] the exploration of which is still at its infancy and demands more focus. By alleviating the interfacial ionomer confinement through engineering ionomer–catalyst/substrate interfaces, we can create more favorable ion transport pathways through thin ionomer layer to ionomer–catalyst interfaces, improve the utilization of expensive catalysts (used Pt majorly), reduce the need for high loading of expensive catalysts, and reduce PEMFC costs, thereby.

In PEMFCs, not only the catalysts are expensive, but also the ionomers used are expensive. Currently, fluorocarbon-based and expensive ionomer, Nafion is used in the membrane and catalyst binder layer. While Nafion conducts protons efficiently in bulk membranes, it offers low thin-film proton conductivity.[23,29,33,34] This demands new design of ionomers which can conduct protons efficiently within thin layers at catalyst/substrate interfaces. The current reality is: ionomer design has received a great deal attention to improve membranes further. However, ionomers are rarely designed to address the challenges of catalyst-binding thin ionomer layers. Instead, ionomers are primarily designed with membrane separator issues in mind,[35–41] and then used for binder applications as well. By designing new ionomers, if the proton conductivity within thin layers can be improved, we can achieve higher ORR efficiency with thinner ionomer layers and low catalyst loading which can cut down the costs of PEMFCs. Moreover, the environmental and health concerns of perfluorinated substances (PFAS) jeopardize the use of perfluorinated ionomers, like Nafion, in the long run. If some of the new ionomer designs can tackle cost and environmental issues, we could simultaneously address performance, cost, and sustainability challenges.

We have dedicated our efforts to these endeavors over the past 15 years realizing the gaps between current states and ultimate technical needs of PEMFCs, Over the time, we adopted a three-pronged approach with a theme "Unravel-Engineer-Design" (Fig. 1d). In this feature article, we summarized our significant contributions in these three key areas: (i) unravel the proton-conduction and other relevant properties of ionomers within sub-μm thick films as well as at ionomer–substrate or ionomer–catalyst interface; (ii) engineer the ionomer–catalyst interface to boost ionic conductivity of thin films; and (iii) design novel ranges of ionomers to address specific interface-related challenges. While highlighting our efforts, we have also integrated relevant work by others to explain and support our observations, providing adequate context.

UNRAVEL ionomer behavior in sub-μm thick films and at ionomer–substrate/catalyst interfaces

Ionomers exhibit weaker ion conductivity in thin films as compared to bulk membranes

Ionomers, in general, behave very differently in sub-μm thick films as compared to several tens of μm thick bulk membranes. Especially in PEMFCs, the ion transport limitation in thin catalyst binder layers, made of traditional ionomers, has been a common scenario.[14,19] Most of the studies to unravel the ion transport limitation have been done with Nafion (Fig. 2a), a fluorocarbon-based ionomer that is the current state-of-the-art proton conducting ionomer. A consistent finding by several groups is that proton conductivity is much weaker in sub-μm thick Nafion films as compared to several tens of μm-thick bulk Nafion membranes. As the thickness of ionomer films decreased, proton conductivity decreased. Yasuda[42] and Karan[43] both developed Arrhenius plots showing higher activation energy or barrier for proton conduction for thin Nafion films than bulk materials. For instance, the activation energy of proton conduction for ∼50 μm-thick bulk Nafion membrane was 15 kJ mol^{-1}, while it was 32 kJ mol^{-1} for ∼50 nm thick Nafion films at 85% RH.[42,43] As the relative humidity (RH) decreased, this activation energy elevated further: 32 kJ mol^{-1} (85% RH); 50 kJ mol^{-1} (60% RH), indicating weaker proton conductivity at low %RH.

The difference in proton conductivity between thin Nafion film and bulk Nafion membrane may vary based on the film deposition technique, but the decrease in proton conductivity with film thickness is a commonly observed phenomenon. Weber, Karan and coworkers (including Dishari) studied the behavior of sub-μm thick, self-assembled Nafion films (4–300 nm thick).[45,47] A 20 nm thick, self-assembled Nafion film offered a proton conductivity of ∼20 mS cm^{-1}, while it was ∼93 mS cm^{-1} for bulk Nafion membrane.[47] Yasuda et al.[42] showed that the proton conductivity of a 100 nm thick drop-cast Nafion film was an order of magnitude lower than a ∼1000 nm (1 μm) thick Nafion film. We unraveled proton conduction and other properties relevant to its hydration environment within spin-coated Nafion films[23,29,48] (Table 2 and Fig. 2). We chose spin-coating to deposit ionomer films as
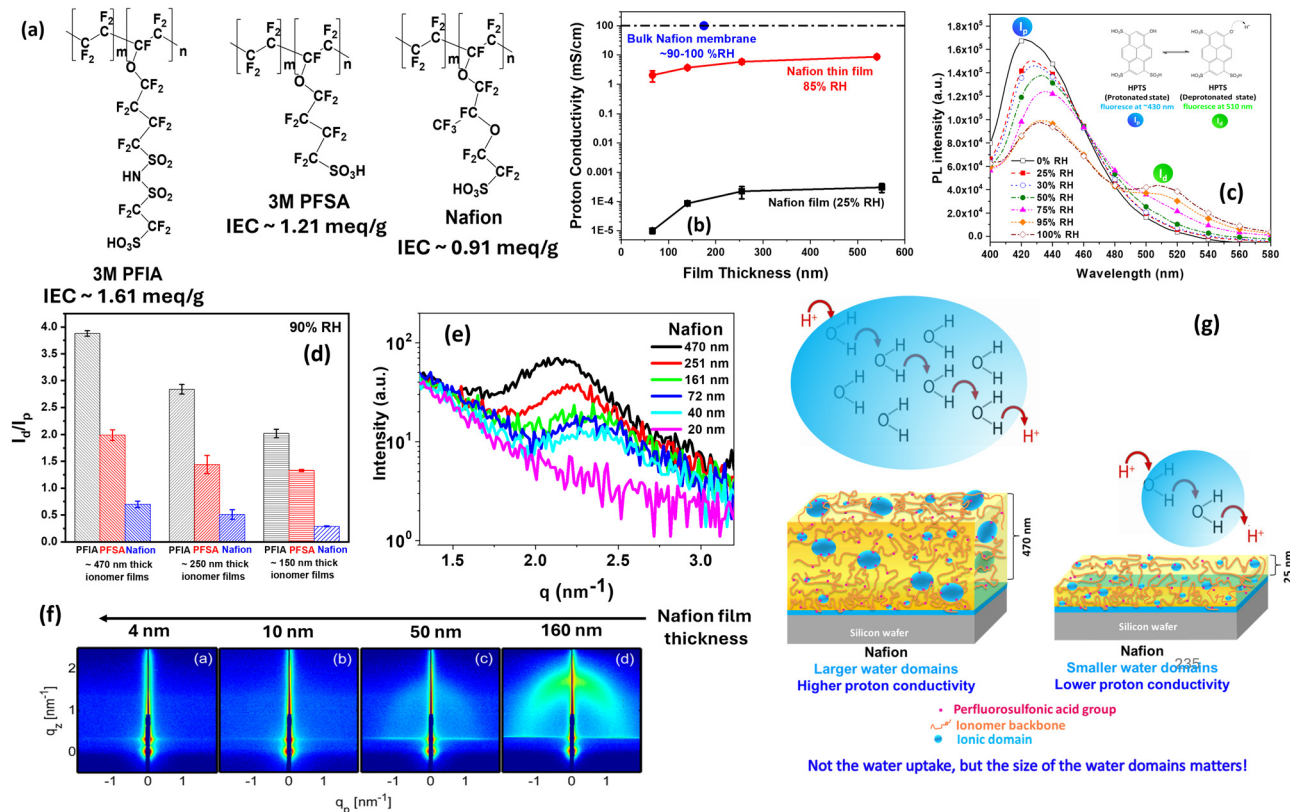
Fig. 2 (a) Chemical structure of 3M PFIA, 3M PFSA and Nafion.[44] (b) Proton conductivity (σ) of Nafion thin films[29] and bulk membranes.[45,46] (c) Working principle of photoacid dye, 8-hydroxypyrene-1,3,6-trisulfonic acid trisodium salt (HPTS) (inset), fluorescence response of HPTS incorporated within a $\sim$590 nm thick Nafion films.[24] Here, I_d and I_p are the emission intensities of HPTS at deprotonated ($\lambda_{em,max} \sim 510$ nm) and protonated ($\lambda_{em,max} \sim 430$–440 nm) states, respectively. (d) I_d/I_p response of HPTS in 3M PFIA, 3M PFSA and Nafion thin films.[44] (e) 0D GISAXS (or RSAXS) profile of Nafion films with different thickness at $\sim$56%RH.[44] (f) 2D GISAXS patterns of Nafion films with different thickness equilibrated at 100% RH.[47] Here, q_p and q_z refer to in-plane and out-of-plane scattering vectors, respectively. (g) Schematic representation of ionic domain characteristics of thick and thin Nafion films.[44] If the ionic domains are small, scattered, and poorly connected, ionic conduction will be weak irrespective of the level of water uptake. Figures regenerated by taking data from ref. 24 and 44–47. Figures reproduced with permission from ref. 44 and 47. Copyrights 2013, 2019, American Chemical Society. Copyright 2002, 2014 The Electrochemical Society.

this is the fastest coating method giving uniform thin films and is widely accepted. We found that proton conductivity (σ) of a $\sim$550 nm thick, annealed Nafion film was 8.67 mS cm^{-1} at $\sim$85% RH.[29] This σ value dropped to 5.90 mS cm^{-1} for 250 nm thick Nafion films, and 2 mS cm^{-1} for 65 nm thick Nafion films (Fig. 2b).[29] These thin-film proton conductivity values were 1–2 orders of magnitude lower than a 25–50 μm thick bulk, freestanding Nafion membranes (80–100 mS cm^{-1} (water vapor);[45,46,49] 131 mS cm^{-1} (liquid water)[23]) Lowering relative humidity reduced proton conductivity significantly: 5.90 mS cm^{-1} (85% RH) vs. 2.2×10^{-4} mS cm^{-1} (25% RH) for 250 nm thick annealed Nafion films (Fig. 2b).[29] Together the low film thickness and low %RH had a far more detrimental effect on thin-film proton conductivity: (σ) 25% RH: 2.2×10^{-4} mS cm^{-1} (250 nm thick Nafion film) vs. 1.04×10^{-5} mS cm^{-1} (65 nm thick Nafion film) (Fig. 2b).[29]

This several-orders-of-magnitude lower proton conductivity (σ) of sub-μm thick Nafion films as compared to several tens of μm thick bulk membranes is thought-provoking, and is attributed to confinement effect. When the film thickness approaches a few multiples of the radius of gyration of its polymer chains, the chains begin to experience geometric

confinement.[51–54] Geometric confinement is an outcome of physical entrapment of polymer chains as they are compelled to stay in low-dimension systems. The confinement effect is magnified further by interfacial interactions and interfacial processes,[14,24,29,55–66] especially in the hydrated ionomer films. The water–ionomer–substrate interfacial interactions can pin the water and ionomers to the substrate/catalyst. Such interfacial confinement[64] alongside geometric confinement[54] can govern ionomer thin film behavior, making it distinctly different from bulk membranes. To be more specific, water–polymer confinement can severely affect the glass transition temperature (T_g),[67–69] hydration behavior,[24,55] water–polymer mobility,[55,70] morphology,[44,70] phase separation,[44,71] nanoscale structural orientation,[61,72] and proton conductivity[47,72] thereby of hydrated ionomer films. Moreover, due to the interfacial processes, thin films end up having heterogeneous microenvironment, unlike bulk ionomer membranes.[25] The heterogeneity, such as mass/density distribution of water–polymer across the thin film[15,58,63,73–78] could lead to a distribution of glass transition temperature,[67–69] water-ionomer mobility[25,75] and proton conductivity[23,25,29,48] across films. To gain a better understanding of thin-film proton conductivity, it is thus

Table 2 Proton conductivities of perfluorinated ionomers in thin films deposited and processed under different conditions

Ionomer	Substrate	Electrode	Film deposition strategy	Film annealing condition	d (nm)[a]	% RH	λ_w[a]	$(T)_\sigma$[a]	σ (mS cm^{-1})[a,b]	Ref.
Nafion	MgO	IDE of Au	Spin coating	Unannealed	60	60	—	25	3.98×10^{-4}	33
						90			1.58	
					400	60			10^{-2}	
						90			2.51	
Nafion	Pt-deposited SiO$_2$	IDE of Au	Spin coating	Unannealed	22	40	—	25	5×10^{-2}	34
						95			12.59	
					360	40			1×10^{-1}	
						95			31.62	
Nafion	SiO$_2$ (with thermal oxide layer)	IDE of Au	Spin coating	Unannealed	22	40	—	25	1.5×10^{-3}	49
						95			6.30	
					400	40			3.1×10^{-2}	
						95			20	
Nafion	SiO$_2$ (with thermal oxide layer)	IDE of Au	Spin coating	Unannealed	30	20	0.5	30	10^{-3}	
						90	4		32	
						20	0.8	80	10^{-2}	
						90	6.3		75	
3M PFSA [EW: 825]	SiO$_2$ (with thermal oxide layer)	IDE of Au	Spin coating	Unannealed		20	0.8	80	10^{-2}	
						90	5.8		60	
3M PFIA [EW: 620]	SiO$_2$ (with thermal oxide layer)	IDE of Au	Spin coating	Unannealed		20	1	80	0.2	
						90	8.3		100	
Nafion	SiO$_2$ (with 200 nm thermal oxide layer)	IDE of Au	Spin Coating	Unannealed	15	21	11	23	3.9×10^{-4}	23
						83	15		3.19	
					100	27	5		8.0×10^{-2}	
						84	10		8.31	
Nafion	SiO$_2$ (with 200 nm thermal oxide layer)	IDE of Au	Spin coating	Annealed	60	24–28	0.07	25	1.2×10^{-5}	29
						83–86	1.1		1.97	
					100	24–28			2.7×10^{-5}	
						83–86			2.83	
					400	24–28			2.60×10^{-4}	
						83–86			7.57	
					550	24–28			2.97×10^{-4}	
						83–86			12.4	
Nafion	SiO$_2$ (with 300 nm thermal oxide layer)	IDE of Au	Self-assembly	Unannealed	10	20	—	60	2.44×10^{-3}	50
						96			94.86	
				Annealed		20			1.2×10^{-4}	
						96			1.2	
Nafion	SiO$_2$/Si wafer	IDE of Au	Self-assembly	Unannealed	4	20	—	25	1.41×10^{-4}	45
						95			24.49	
					160	20			3.46×10^{-1}	
						95			44.72	

[a] d: film thickness, λ_w: hydration numbers, $(T)_\sigma$: temperature at which proton conductivity was measured, σ: proton conductivity. [b] All proton conductivities are measured in-plane direction.

critical to gain a systematic understanding of the film thickness effect on the aforementioned average and distributed properties.

Fluorescence can be a powerful tool to unravel ionomer thin film properties

We made a significant contribution to understanding the proton conduction environment within ionomer thin films by developing and extensively using a range of fluorescence-based strategies (Fig. 2c, d, g, Fig. 3b, d, Fig. 4d–f, Fig. 5, Fig. 6c, Fig. 9d and Fig. 10d). Fluorescence-based techniques, considering qualitative, are often ignored. But they can reveal a wealth of information about polymer membranes and thin films, such as glass transition temperature,[79–83] aging,[80,82,84] ion transport dynamics,[85–88] structural/orientational relaxation dynamics,[89,90] and mobility.[91]

For instance, by staining ionomer films with fluorescent photoacid dyes, we were able to measure the extent of proton conduction (deprotonation ratio), local proton concentration and pH within ionomer films. We also showed that the deprotonation ratios nicely complement the quantitative values of proton conductivity (σ), measured using electrochemical impedance spectroscopy (EIS) (Fig. 2d *vs.* Fig. 2b, discussed in detail in the next section), validating the reliability of fluorescence-based techniques. In fact, fluorescence offered insights that traditional thin-film characterization methods could not. For example, we revealed both average[24,29,47,70] and location-/depth-specific[23,25,29,48] proton conduction behavior across ionomer films. These are unique information for the energy research community and especially valuable for ionomer thin films whose properties can vary significantly at different interfaces, unlike free-standing bulk membranes. In our work, we particularly stained ionomer films with fluorescent dyes sensitive to local pH, proton concentration, extent of proton conduction and mobility, and leveraged steady state fluorescence spectroscopy, time-resolved fluorescence spectroscopy, and confocal laser scanning microscopy (CLSM) to investigate key properties. The goal was to understand the water–polymer mobility,[24,55,70,75] ionic domain characteristics,[44,70] hydration-induced plasticization,[24,25,55,70,75] and average-[24,29,47,70] and distributed[23,25,29,48] proton conduction behavior[23–25,29,47,48,70] across ionomer films. We also performed traditional morphological, mechanical, and electrochemical characterizations simultaneously, combining these with observations from fluorescence-based techniques to better understand what happens under thin film confinement. We extended this combined approach to a wide range of fluorocarbon- and hydrocarbon-based ionomers. This feature article captures some of our key observations so far about ionomer thin films through these attempts.

Fluorescent photoacid dyes can reliably inform about local proton conduction environment and help understand quantitative values of proton conductivity (σ)

We stained a series of sub-μm thick ionomer films with a fluorescent photoacid dye, 8-hydroxypyrene-1,3,6-trisulfonic acid trisodium salt (HPTS) and exposed the films to different %RH[23,24,44,48] to probe the change in proton conduction environment. HPTS has a phenolic –OH group that responds to local proton concentration *via* protonation/deprotonation (Fig. 2c, inset). At dry or low humid state, the phenolic –OH does not dissociate and emits blue fluorescence (I_p) from its protonated state. But when the film is hydrated and the surrounding hydration environment of HPTS becomes favorable for proton conduction, HPTS donates its phenolic proton (–OH $\leftrightarrow$ –O$^-$ + H$^+$), and the proton is carried away from the proton generation site by water molecules and ionomer's ion-conducting groups. The deprotonation of HPTS in a strongly proton-conducting environment thus emits green fluorescence (I_d). The ratio of green-to-blue fluorescence (I_d/I_p) from HPTS gives an indirect measure of extent of proton transport. We observed that I_d/I_p increased with the increase in %RH (Fig. 2c) and film thickness (Fig. 2d).

σ, on the other hand, is the typical measure of quantitative value of proton conductivity, obtained using EIS. We revealed that σ and I_d/I_p scales with each other and give complementary information. Just like we saw a decrease in proton conductivity (σ, Fig. 2b), we saw a decrease in I_d/I_p ratio as the Nafion films became thinner (Fig. 2d). For instance, I_d/I_p of Nafion film decreased from 0.70 to 0.29 as the film thickness decreased from 470 nm to 150 nm (Fig. 2d),[44] while σ decreased from 8.18 mS cm^{-1} to 3.89 mS cm^{-1} for Nafion films with similar thickness (Fig. 2b).

Proton conduction environment in fluorocarbon and traditional hydrocarbon-based ionomers can be different

We extended the developed HPTS-based technique to study thin film behavior of a series of perfluorinated ionomers: 3M PFIA, 3M PFSA and Nafion (Fig. 2a).[44] We observed that I_d/I_p decreased as the ionomer film thickness decreased irrespective of the type of ionomer studied. Also, the I_d/I_p of HPTS embedded within ionomer films followed the trend: 3M PFIA > 3M PFSA > Nafion (Fig. 2d), similar to what was reported for these ionomers in bulk membranes.[39,93,94] While there can be various influencing factors, the proton conductivity trends of these three ionomers aligned with the expected impact of ionomer chemical structure on proton conduction. 3M PFIA, 3M PFSA and Nafion have the same fluorocarbon-based backbone, but their side chains are not the same. All of them have one perfluorosulfonic acid (–CF$_2$SO$_3$H)-based proton-conducting group per side chain, while 3M PFIA has an additional proton-conducting group, bis sulfonyl imide (R$_f$–SO$_2$–NH–SO$_2$–R$_f$). The Gibbs free energy of acid dissociation (also known as gas-phase acidity) of bis sulfonyl imide group (ΔG_{acid} = 284.1 kcal mol^{-1})[95] is lower than perfluorosulfonic acid (ΔG_{acid} = 299.5 kcal mol^{-1}).[95] With two proton-conducting groups per side chain, including one highly acidic, 3M PFIA thus emerged as the strongest proton conductor in this fluorocarbon-based ionomer series, as reflected in the I_d/I_p values, even under thin-film confinement[44] (Fig. 2d).

To avoid toxic perfluoro substances and cut down ionomer costs, hydrocarbon-based ionomers are designed. However, sulfonated polysulfone (sPSf), a leading hydrocarbon-based ionomer, exhibited negligible green fluorescence (I_d) and the lowest I_d/I_p ratio,[96] matching with its low thin-film proton conductivity (σ: 9 mS cm^{-1} (Nafion) *vs.* 0.2 mS cm^{-1} (sPSf), 150 nm thick unannealed films on Au/SiO$_2$, 85%RH).[48]

Table 3 Summary of hydrocarbon-based ionomer performances reported for cathode catalyst layers or membrane electrode assemblies (MEAs)

Membrane ionomer[b]	Cathode binder ionomer[b]	Binder ionomer IEC[a] (meq g⁻¹)/DS (%)	Binder ionomer content (wt% or mg cm⁻²)	Binder ionomer/carbon ratio (I/C)	Cathode catalyst loading (mg cm⁻²)	Cathode catalyst/support (wt ratio)	Operating conditions	Current density at 0.7 V[c] (A cm⁻²)	Power density at 0.7 V[c] (W cm⁻²)	Ref.
Nafion	Nafion	n.a.[a]	n.a.	—	0.05 / 0.1 / 0.2	PtCo/C	94 °C, H₂/air, 65% RH, 2.47 atm	1.125 / 1.25 / 1.65	0.78 / 0.875 / 1.16	8 and 105
Nafion	Nafion	n.a.	n.a.	—	0.05 / 0.1 / 0.2	PtCo/C	80 °C, H₂/air, 100% RH, 1.48 atm	0.7 / 1 / 1.2	0.49 / 0.7 / 0.84	8
Nafion 211	Nafion D520	1/—	30 wt%	—	0.4	Pt/C	80 °C, H₂/O₂, 100% RH, 1 atm	0.85	0.595	36
Nafion 211	sPEEK	1.4/—	30 wt%	—	0.4	Pt/C (46/54)	80 °C, H₂/O₂, 100% RH, 1 atm	0.115	0.081	102
Gore M735.8	Nafion D2021	0.92/—	28 wt%	—	0.4	Pt/C (40/60)	80 °C, H₂/air, 100% RH, 1 atm	0.47	0.33	106
PFSA 1050 EW[a]	PFSA 1050 EW	0.95/—	31 wt%	—	0.4	Pt/C (40/60)	80 °C, H₂/O₂, 75% RH, 1 atm	0.18	0.126	19
PFSA 750 EW	PFSA 750 EW	1.33/—	31 wt%	—				0.2	0.14	
Nafion 112	sPEEK 550 W	1.8/—	31 wt%	—				0.02	0.014	
PFSA 750 EW	PFSA 750 EW	1.33/—	24 wt%	—				0.2	0.14	
Nafion 112	sPEEK 750 EW	1.33/—	15 wt%	—				0.075	0.053	
Nafion 112	sPSU 650 EW	1.54/—	15 wt%	—				0.06	0.042	
sPEEK (IEC 1.75)	Nafion	0.91/—	30 wt%	—	0.4	Pt/C	80 °C, H₂/air, 75% RH, 1 atm	0.05	0.035	21
	sPEEK	1.35/—						0.022	0.015	
		1.75/—						0.022	0.015	
		2.1/—						0.04	0.028	
Nafion 112	Nafion 112	0.91/—	n.a.	—	0.2	Pt/C (20/80)	60 °C, H₂/O₂, 75% RH, 1 atm	0.3	0.21	107
	sPSU-P50	0.95/—						0.2	0.14	
sPEEK	Nafion	0.91/—	45 wt%	—	0.4	Pt/C (40/60)	75 °C, H₂/air, 100% RH, 1 atm	0.25	0.18	99
	sPEEK	1.74/—	40 wt%	—				0.185	0.13	
	sPEEK	1.74/—	10 wt%	—				0.1	0.07	
Nafion 112	Nafion	0.91/—	30 wt%	—	0.48	Pt/C (60/40)	65 °C, H₂/air, 100% RH, 1.4 atm	0.4	0.28	98
Nafion 112	sPEEK	1.88/65	30 wt%	—	0.3	Pt/C (60/40)	65 °C, H₂/air, 100% RH, 1 atm	0.12	0.084	101
Nafion 112	sPEEK	—/60						0.095	0.067	
sPEEK (IEC 1.9)	Nafion	0.91/—	30 wt%	—	0.25	Pt/C (20/80)	50 °C, H₂/O₂, 100% RH, 1 atm	0.3	0.21	103
	sPEEK	1.9/—	10 wt%	—				0.14	0.098	
	sPEEK	1.9/—	30 wt%	—				0.14	0.098	
	sPEEK	1.9/—	40 wt%	—				0.05	0.035	
sPEKK (IEC 1.4)	Nafion	1.4/—	25 wt%	—	0.4	Pt/C (45.8/54.2)	80 °C, H₂/O₂, 75% RH, 1 atm	0.625	0.44	108
Nafion 112	sPE	1.61/—	—	0.7 I/C	0.5	Pt/C (45.8/54.2)	50 °C, H₂/O₂, 100% RH, 1 atm	0.5	0.35	109
		2.17/—						0.54	0.38	
		3.73/—						0.24	0.17	
Nafion 117	Nafion	0.91/—	30 wt%	—	0.25	Pt/C (20/80)	35 °C, H₂/air, 100% RH, 2.04 atm	0.058	0.04	100
	sPEEK	1.88/67						0.013	9.1×10^{-3}	
Nafion 112	sPE	1.61/—	—	0.7 I/C	0.5	Pt/C (45.8/54.2)	70 °C, H₂/O₂, 100% RH, 1 atm	0.225	0.16	109
		2.17/—						0.34	0.24	
		3.73/—						0.275	0.19	
Nafion 112	sPE	2.17/—	—	1 I/C	0.5	Pt/C (45.8/54.2)	70 °C, H₂/O₂, 100% RH, 1 atm	0.26	0.18	109
Nafion 117	Nafion	1.59/—	0.9 mg cm⁻²	—	n.a.	n.a.	70 °C, H₂/O₂, 100% RH, 1 atm	0.5	0.35	104
sPES-40	sPES-40						70 °C, H₂/O₂, 100% RH, 3 atm	0.3	0.21	

Table 3 (continued)

Membrane ionomer[b]	Cathode binder ionomer[b]	Binder ionomer IEC[a] (meq g⁻¹)/DS (%)	Binder ionomer content (wt% or mg cm⁻²)	Binder ionomer/carbon ratio (I/C)	Cathode catalyst loading (mg cm⁻²)	Cathode catalyst/support (wt ratio)	Operating conditions	Current density at 0.7 V[c] (A cm⁻²)	Power density at 0.7 V[c] (W cm⁻²)	Ref.
Nafion 112	sPAE	2.5/— 2.5/— 1.8/—	—	0.7 I/C	0.5	Pt/C (48/52) Pt/C (68/32) Pt/C (68/32)	80 °C, H₂/O₂ 100% RH, 1 atm	0.15 0.25 0.2	0.105 0.175 0.14	110
Nafion 212 sPAES PES	BPS-27k BPS-27k	n.a.	20 wt%	—	0.4	Pt/C (46.2/53.8)	80 °C, H₂/O₂ 100% RH, 1 atm	0.5 0.3	0.35 0.21	111 and 112
PES	PES	1.43/—	2 wt% 32 wt%	—	0.4	Pt/C (40/60)	70 °C, H₂/O₂ 100% RH, 1 atm	0.115 0.025	0.081 0.018	113
F-PES	F-PES	1.28/—	2 wt% 32 wt%	—	0.4	Pt/C (40/60)	70 °C, H₂/O₂ 100% RH, 1 atm	0.1 0.06	0.07 0.042	113
sPPP	sPPP	2.17/— 3.70/—	20 wt%	—	0.4	Pt/C	80 °C, H₂/O₂ 100% RH, 1 atm	0.13 0.74	0.091 0.518	114
sPPB	sPPB	3.23	7.5 wt%		0.4	Pt/C (46.5/54.5)	80 °C, H₂/O₂ 100% RH, 1 atm	0.8	0.56	115
sPPB	sPPB	3.19/—	15 wt% 30 wt%	—	0.4	Pt/C	80 °C, H₂/O₂ 100% RH, 1 atm	0.65 0.25	0.455 0.175	22
Nafion 112	sPI		n.a.	0.5	0.5	Pt/C (46.3/53.7)	70 °C, H₂/O₂ 100% RH, 1 atm	0.4	0.28	116
NEXAR	NEXAR	1	33 wt%	—	0.52	Pt/C (66.7/33.3)	80 °C, H₂/O₂ 100% RH, 1 atm	0.25	0.18	117
Pemion	Pemion	3.1	9 wt%	0.2 I/C	0.4	PtCo/C (45.3/54.7)	80 °C, H₂/O₂ 95% RH, 2.47 atm 80 °C, H₂/air 95% RH, 2.47 atm	1.25 0.6	0.875 0.42	118
Nafion® 212	Spiro 30	29.1	5 wt%		0.4	Pt/C (46.5/53.5)	65 °C, H₂/air 95% RH, n.a.	0.035	0.02	119
Nafion 212	Nafion SDT COF-Nafion	1 1.70 (COF)/—	n.a.	0.8	0.07	Pt/C (40/60)	80 °C, H₂/O₂ 95% RH, 2.47 atm	0.5 1.5	0.35 1.05	120
Nafion 212	Nafion SDT COF-Nafion	1 1.70 (COF)/—	n.a.	0.8	0.07	Pt/C (40/60)	80 °C, H₂/air 95% RH, 2.47 atm	0.25 0.5	0.175 0.35	120
U.S. DOE Target			≤ 0.3 (2030); ≤ 0.25 (2050)³					1.07 (2023)⁵ 3–4 (2030)9	1.8 (2025)^[10,11] > 2 (2030)^[9,10]	3,5 and 9–11

[a] n.a. = information not available; EW = equivalent weight = 1000/IEC, where IEC = ion exchange capacity. [b] PFSA= perfluorosulfonic acid, sPEEK = sulfonated poly(ether ether ketone), sPEKK = sulfonated poly (ether ketone ketone), sPE/sPSU/sPAE/sPES/sPAES/BPS = derivatives of sulfonated poly (arylene ether sulfone), sPPP = sulfophenylated poly(phenylene), sPPB = sulfophenylated poly(phenylene) biphenyl, PES = sulfonated poly (ether sulfone), F-PES = fluorinated poly (ether sulfone), sPI = derivatives of sulfonated polyimide, Nexar = sulfonated styrene-based pentablock terpolymer, Pemion = derivative of sulfophenylated poly(phenylene), Spiro = derivative of poly(arylene ether sulfone) containing spirobiindane groups. [c] Current and power densities are reported at 0.7 V because a fuel cell typically generates a voltage from 0.6–0.7 V at a full-rated load.

Overall, these I_d/I_p – σ studies revealed that commonly known ionomers (both fluoro- and hydrocarbon-based) conduct protons poorly in thin films. Additionally, some of the well-known hydrocarbon-based ionomers (e.g., sulfonated poly(ether ether ketone) (sPEEK), sulfonated poly(sulfone) (sPSf)), conducting proton efficiently in bulk membranes,[97] fail badly to conduct protons in sub-μm thick films. This negatively impacts the performance (current density, power density, ORR kinetics) in membrane electrode assemblies (MEAs) (Table 3).[18–22,98–104] Understanding why these occur is crucial for improving electrode design and ORR efficiency. After being barely touched for decades, understanding in this area is now gradually evolving. In this section, we briefly discussed the effect of the chemical structure of ionomers, but there are many other factors that impact the thin-film proton conductivity in a complicated manner. We thus put efforts into identifying those other factors responsible for poor proton conductivity in thin films.

Ionic domain size and connectivity matter more than water uptake

A common school of thought is higher water uptake should lead to higher proton conductivity. The reason is water facilitates proton hopping. However, our study of hydration number (λ_w, moles of water/moles of proton-conducing groups) of ionomer thin films revealed something interesting. We repeatedly showed for many ionomers that there is no straightforward correlation between hydration number (λ_w) and proton conduction behavior (I_d/I_p and σ) of ionomer thin films.[23,24,44,48] For instance, a 70 nm thick Nafion film showed λ_w similar to a 50 μm thick bulk Nafion membrane.[24] However, the I_d/I_p value was an order of magnitude lower in the thin film as compared to the bulk membrane.[24] These facts indicated that there may be factors other than water uptake which control the proton conduction in sub-μm thick, confined ionomer films.

We found that thinner, spin-coated films of fluorocarbon-based ionomers (3M PFIA, 3M PFSA, Nafion) had higher degree of phase mixing from TEM images.[44] Also, thinner films did not show any significant scattering, suggesting a loss of correlation between ionic domains in the polymers in both 0D-GISAXS (Fig. 2e)[44] and 2D-GISAXS[47] studies (Fig. 2f). We generated a calibration curve showing I_d/I_p response of HPTS in aqueous solutions with different acid (HCl) concentration and used this curve to predict the proton concentration in HPTS-stained films of 3M PFIA, 3M PFSA and Nafion by comparing the I_d/I_p values.[44] A similar method was adopted earlier to understand membranes by Fayer et al.[121] What we found was that as the film thickness and %RH decreased, proton concentration ([H⁺]) in the ionic domains increased suggesting protonic confinement within ionic domains and poor connectivity between ionic domains.[44] Later, by comparing the I_d/I_p response of HPTS in reverse micelles and ionomer films, we found that the average size of ionic domains in sub-μm thick ionomer film ($\sim$1–2 nm) is smaller than that in bulk membranes (4 nm).[44] Moreover, the size of ionic domains in films of all three ionomers, independently obtained from RSAXS and steady-state fluorescence, closely matched.

Together these facts tell a story. Proton transport requires long-range, connected pathways achievable through the formation of well-connected, large hydrophilic phases or ionic domains. In an ideal scenario, proton conduction happens through the Grotthuss mechanism, where water molecules form H-bonded network to create a continuous pathway for proton hopping. However, if the ionic domains are small, scattered, and ill-connected (as seen in TEM, GISAXS, fluorescence studies), ion hopping, and ionic conduction weakens despite high water uptake (Fig. 2g). This is likely what happens in thinner Nafion and other fluorocarbon ionomer films and explains their weak proton conductivity in thin films. The hydrophilic–hydrophobic phase mixing and disconnect between ionic channels in thin films could be far more severe in hydrocarbon-based ionomers explaining why traditional hydrocarbon-based ionomers exhibit conductivity[48,96,118] much lower than fluorocarbon-based Nafion. For instance, the in-plane proton conductivity of the binder phase was reported as 10 mS cm⁻¹, 1.12 mS cm⁻¹ and 0.7 mS cm⁻¹ when PFSA, sPEEK, and sPSf were used as binder ionomer, respectively.[19] This also explains why traditional hydrocarbon-based ionomers suffer more from catalyst binder-phase diffusion limitation,[18,19] sluggish ORR kinetics,[103,104] and lower power density[20] compared to fluorocarbon-based MEAs (Table 3, power density at 0.7 V). For example, at $\sim$30 wt% ionomer loading in Pt/C-based binder phase, the power density of MEA at 0.7 V was reported as 0.60 W cm⁻² for Nafion (membrane)-Nafion (binder),[36] whereas 0.08 W cm⁻² for Nafion (membrane)-sPEEK (binder)[102] at comparable conditions (80 °C, H₂/O₂, 100%RH, 1 atm).

Kreuer[122,123] and later Holdcroft[118] held similar factors (less acidic side chains, poor phase segregation, narrower and less connected ionic channels with more dead ends) responsible for explaining the weaker transport behavior of hydrocarbon-based ionomers than fluorocarbon-based ionomers even in bulk membranes at low humidity conditions, where also protonic confinement is obvious. These findings suggested that controlling the size and connectivity of ionic domains is crucial for improving thin film ionic conductivity.

Polymer chains and water molecules are pinned to the substrate and lose mobility in thin films

Another important observation we made is that ionomer chain and water mobility are sacrificed in thin films. This is a combined effect of both thin-film confinement and interfacial interactions. The thin-film confinement effect was evident when the mobility or stiffness of bulk, free-standing Nafion membrane was compared with a sub-μm thick Nafion film on the substrate. This was effectively probed by staining Nafion samples with a rotor probe (9-(2-Carboxy-2-cyanovinyl)julolidine, CCVJ), the green fluorescence of which intensifies when it resides in a stiff or less mobile environment (Fig. 3a). As can be seen, a 70 nm thick Nafion film experienced hydration-induced antiplasticization or stiffening at 25–30% RH (i.e. $(I_{RH}/I_0)_{25–30\% RH} > (I_{RH}/I_0)_{dry state}$). In contrast, a 25 μm thick Nafion membrane did not show any sign of antiplasticization, rather the film softened over the entire humidity range (Fig. 3b).[24,55] The stiffening of thinner films was in agreement with the modulus
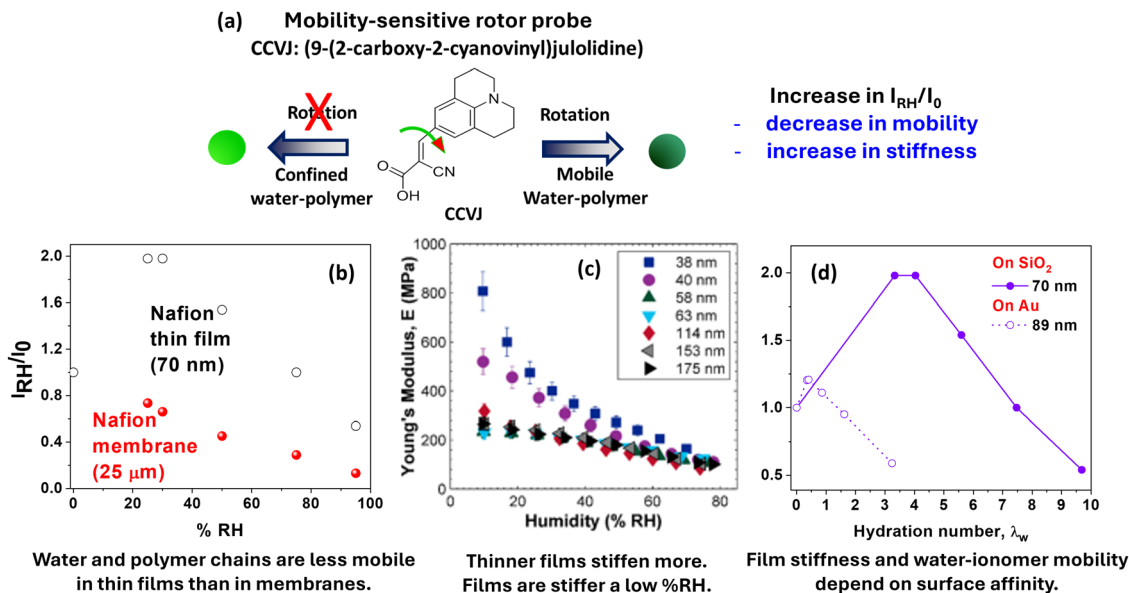
Fig. 3 (a) Working principle of CCVJ. The green fluorescence of CCVJ increases as it resides in a stiff environment. I_{RH} and I_0 means fluorescence intensity of CCVJ at a certain %RH and dry state, respectively. An increase in I_{RH}/I_0 thus mean a decrease in water–polymer mobility or increased stiffening/antiplasticization of ionomer films upon hydration. (b) Relative fluorescence intensities (I_{RH}/I_0) of CCVJ in a 70 nm thick Nafion film on n-SiO$_2$ substrate and bulk Nafion (NR-212) membrane.[24,55] (c) Young's modulus of Nafion films as a function of film thickness and relative humidity.[92] (d) (I_{RH}/I_0) of CCVJ in a 70 nm thick Nafion film on n-SiO$_2$ and Au substrates.[24] Figures reproduced with permission from ref. 24, 55 and 92. Copyrights 2012, 2013, 2016, American Chemical Society.

data obtained by Soles *et al.* (Fig. 3c),[92] Weber *et al.*[124] and later by us[29,48] where the modulus of Nafion films increased as the films became thinner. Similar hydration-induced stiffening was observed for s-Radel (Fig. 4a) in thin films using CCVJ and time-resolved fluorescence (discussed later, Fig. 4).[75]

Unlike bulk, free-standing, bulk membranes, thinner ionomer films experience a substrate interface. Therefore, the observed stiffness is not only a thickness-induced effect but also induced by ionomer–water interactions with substrate on which thin films were made. For example, a Nafion film made on a highly interactive substrate (*e.g.*, on native oxide of silica (n-SiO$_2$)) sorbed more water and stiffened more than a Nafion film with similar thickness but made on a less-affine substrate (*e.g.* Au) (Fig. 3d).[24] The –SiOH groups of silica-based substrates (with native/thermal oxides) can form H-bonds with –SO$_3$H groups of ionomer side chains and water (H$_2$O). There can also be electrostatic interaction between –SO$_3^-$ groups of ionomers and hydronium ions (H$_3$O$^+$), seen for Nafion films on both SiO$_2$[14,24,55,65,125] and Pt/PtO.[14,56–60,62,63,66,126,127] Such interactions can pin the ionomer chains and water molecules to substrate and limit their mobility in thin films.[24,55] On the contrary, Au has lower affinity to –SO$_3$H and water as compared to SiO$_2$[73] and acts as a less restrictive surface than SiO$_2$ (proven by T_g – studies[64]). The lower magnitude of interaction thus caused less chain pinning to substrate and less stiffening of Nafion films on Au (Fig. 3d). Also, On a relevant note, higher water uptake by films (Nafion[24] or s-Radel[75]) on interactive substrates may be tied to the formation of water-rich layers near the substrate, seen consistently using neutron reflectometry (NR) by Dura,[73–75] Decaluwe,[74,76] Karan,[15,78] Dishari,[75] Inukai,[58,77] Yager,[128] and others[63] (discussed in next section).

Distribution of ionomer chains and water across the film is heterogenous across thin films

In sub-μm thick films, the mass distribution of ionomer and water is not the same across ionomer films. Neutron reflectometry (NR)[58,73–76,128] revealed that in hydrated films, ionomer chains form several nm-thick lamellar layers next to substrates (SiO$_2$, Au, Pt, C) which are often water-rich, and the rest of the film is more bulk-like with random ionomer-water distribution. The number, thickness, and composition of lamellar layers in ionomer thin films were found to be dependent on the nature of ionomer,[15,73–75] film thickness,[74,75] interactive nature[15] and roughness[76] of substrate[58,76,129] on which the films were made, and hydration level. For example, Nafion films are reported to have multiple water- and polymer-rich lamella layer next to thermal SiO$_2$ substrate,[73,74] whereas s-Radel (Fig. 4a) films only had one thin water-rich layer next to substrate (Fig. 4b and c).[75] Karan *et al.*[15] suggested a correlation between ionomer side chain length and thickness of interfacial water layer, whereas DeCaluwe *et al.*[76] showed that hydrophilic and smooth substrate interfaces favored lamellar phase segregation more. Dura, DeCaluwe and co-workers (2018)[74] also showed that the water volume fraction in the interfacial lamellar layer is higher than that in the bulk layer in ≥60 nm thick Nafion films on SiO$_2$. The plausibility of such a scenario was suggested by Dishari and Hickner (2012)[55] from hydration number (λ_w) and rotor probe-based studies (I_{RH}/I_0), *i.e.*, a high volume fraction of water accumulating in lamellar zones next to substrate is likely leading to higher water uptake by thin films and its antiplasticization. Additionally, Hickner (IR, ellipsometry),[61,125] Kusoglu (3D GSAXS),[14,65,66] Notsu (sum frequency generation (SFG) spectroscopy),[77] Lee (simulation)[126] and many others
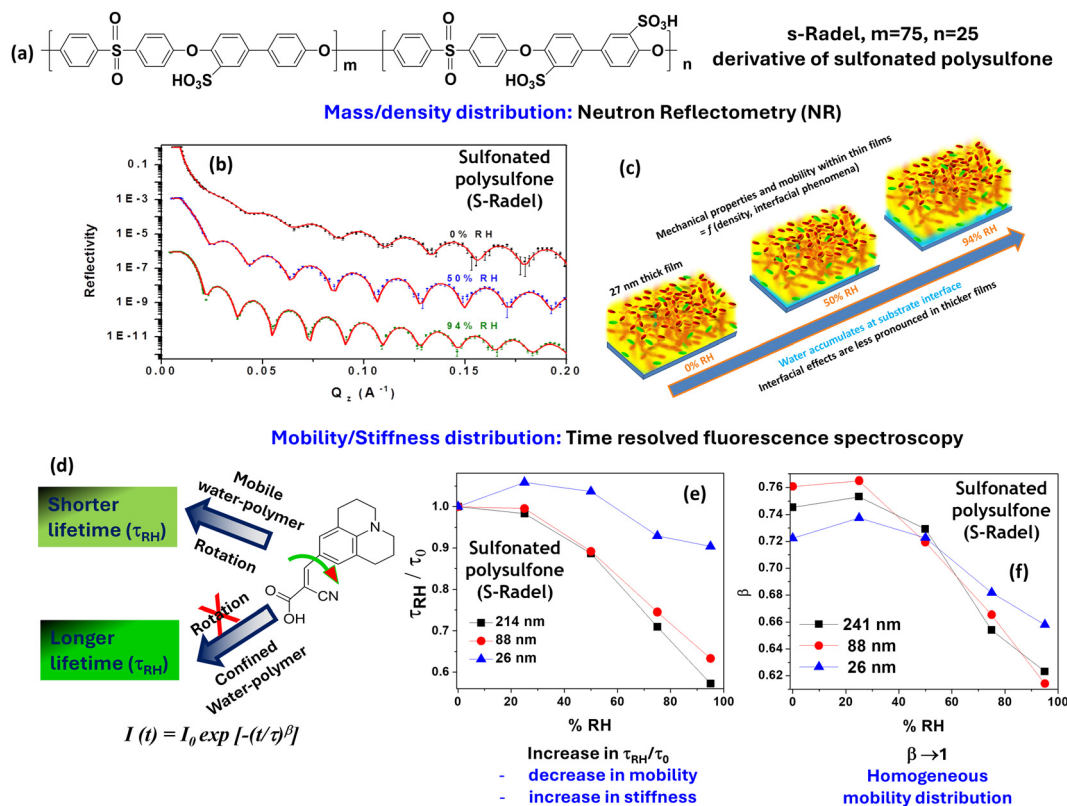
Fig. 4 (a) Chemical structure of s-Radel, a sulfonated poly (phenyl sulfone)-based ionomer. (b) and (c) Neuron reflectometry is used to explore mass and density distribution across ionomer thin films. (b) NR data (symbols) and best model fits (lines in red) for 26 nm thick s-Radel films at different relative humidity conditions.[75] (c) Schematic depicting water accumulation next to substrate interface of s-Radel thin films. (d)–(f) Time-resolved fluorescence spectroscopy of CCVJ-containing s-Radel films revealed that there is a mobility distribution across ionomer films.[75] τ_{RH} and τ_0 represent fluorescence lifetime of CCVJ at certain %RH and dry state, respectively. τ_{RH}/τ_0 indicates the relative change of fluorescence of lifetime (or mobility) at certain %RH with respect to dry state fluorescence lifetime (or mobility). β is a stretching parameter the value of which represents mobility distribution within s-Radel thin films and increased hydration makes the microenvironment more heterogeneous in terms of mobility or stiffness. Figures reprinted with permission from ref. 75. Copyright 2018, American Chemical Society.

(2014-) showed that in the next-to-substrate (SiO$_2$, Pt) region, ionomer (Nafion) chains preferentially orient their backbones parallel to the substrate, while their side chains (–SO$_3$H-terminated) face the substrate. These individual studies supported each other and together suggested that such chain orientation favors interfacial interactions among silanol (–SiOH) groups of substrate, water, and –SO$_3$H groups of Nafion chains lying flat on the surface. As a result, ionomer chains and water get pinned to the substrate,[24,29,55,130–132] lose mobility,[24,55,70,75] and stiffen the films.[24,29,48,55,124,130] Nafion films on Au and Pt also showed heterogeneous water distribution[63] and interfacial water accumulation.[73,126] However, the compositions of interfacial layers in Nafion films on different substrates were different.[73] For example, Au accumulated less water next to it than SiO$_2$. Since water plays a big role in inducing interfacial interaction, Nafion films on Au stiffened less than Nafion films on SiO$_2$ (Fig. 3d).[24]

Average ionomer properties do not tell the full story – thin-film properties can be distinctly different at different depths and interfaces

Understanding of ionomer thin films evolved over time, but took a turning point, when new tools were explored to study distributed

properties, alongside average properties for the entire film. The understanding of depth-specific properties is critical for thin films as unlike bulk systems, thin film behavior can be locally influenced by different interfaces. Especially, many unique processes occur at the ionomer–substrate interface the effect of which can propagate across the film and modulate ionic conductivity and many other properties across the film. For a long time, this aspect of ionomer films remained largely unexplored as traditional ionomer characterization strategies, except a few, give average properties only. Of these few strategies, are neutron reflectometry (NR),[58,73–75,77] X-ray computed tomography (X-ray CT),[133,134] cryo-TEM tomography,[135] and resonant soft X-ray scattering (RSOXS)[136–138] have elucidated the mass/density distribution,[58,73–75,77,133,134] 3-dimensional chemical[136] and nanostructure[134–136] within heterogeneous materials. However, many of these strategies require intense modeling efforts which also require extensive expertise to interpret ionomer properties reliably and meaningfully. On top of that, these instruments are not often accessible for routine, everyday use which is critical for material exploration at nanoscale to expedite energy materials discovery. Fluorescence[79,139,140] and ellipsometric[69] techniques are often employed to unravel the T_g- distribution across polymer thin films. However, ion conduction[45] and
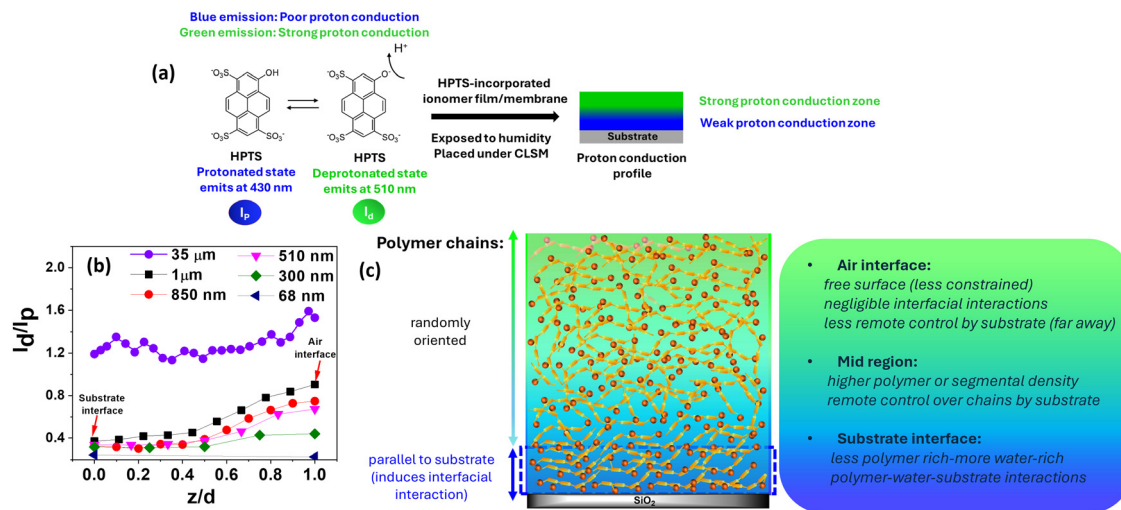
Fig. 5 (a) Schematic representing how incorporating HPTS helps to unravel depth-specific ion conduction in thin films and membranes using CLSM. (b) I_d/I_p profiles for 68–1000 nm thick Nafion films (annealed) on glass coverslips (having SiO$_2$ on the surface) and 35 μm thick free-standing Nafion membrane at 90% RH.[25] Here, z is the distance within the film from the substrate interface, d is the film thickness. The term z/d indicates thickness (d)-normalized distance (z) from the substrate interface. Therefore, z/d values of 0 and 1 signify substrate and air interfaces, respectively. (c) Schematic representing the depth-specific phenomena giving rise to the depth-specific proton conduction environment across Nafion films. (a and b) were reprinted with permission from ref. 25. Copyright 2021, American Chemical Society.

mechanical properties,[92] the two key performance parameters of ionomers, are still reported as an average value for entire samples. Therefore, effective strategies are critically needed to reveal the distribution of these properties across ionomer samples.

Dishari put significant efforts into addressing these needs. In one effort, Dishari et al.[75] revealed time-resolved fluorescence properties of CCVJ incorporated in s-Radel thin films (Fig. 4d–f). A remarkable decay in the lifetime of CCVJ was found for the thicker films at high hydration condition, while it was not the case for thinner s-Radel films (Fig. 4e). This confirmed hydration-induced antiplasticization and higher confinement in thinner s-Radel films. The fluorescence decay of CCVJ in s-Radel film was fitted to a stretched exponential function, where β is a stretching parameter ($0 \leq \beta \leq 1$). β tells about the distribution of fluorescence lifetime (τ). The value of β approaches 1 as the mobility within the hydration environment becomes more homogeneous. Interestingly, as we gradually hydrated s-Radel films, β values moved away from 1 (Fig. 4f) suggesting mobility distribution becoming more and more heterogeneous. This made us realize that there is a distribution of hydration environments across ionomer films and thus proton conduction and other relevant properties can also be heterogeneously distributed across ionomer films. In our work, we thus routinely looked beyond the average properties by developing a robust, everyday-accessible, fluorescence confocal laser scanning microscopy (CLSM)-based technique[23,25,29,48] (Fig. 5).

Proton conduction environment is not the same across ionomer thin films – interfacial effects propagate

We developed a fluorescence confocal laser scanning microscopy (CLSM)-based strategy[23,25,29,48] that can probe the distribution of mobility, ion conduction, and other properties across ionomer

samples. Using CLSM, we were the first to reveal that ionic conduction across ionomer thin films varies along the depth of the films and is highly interface-dependent.[23,25,29,48] To probe the depth-specific proton conduction properties across ionomer thin films and membranes, we incorporated HPTS dye into Nafion thin films and membranes and then placed them under a confocal microscope inside a humidity-controlled chamber. We took multiple xy-plane images at different depth within dry/hydrated ionomer samples. Subsequently, these xy-plane images were z-stacked to obtain a depth profile image representing the fluorescence response of HPTS along the thickness of the ionomer samples (I_d/I_p profile, Fig. 5a and b). This I_d/I_p profile revealed the distribution of proton-conduction environment across hydrated ionomer thin films/membranes.

When we took CLSM images, we observed distinctly different proton conduction behavior (I_d/I_p) across bulk, free-standing Nafion membrane (35 μm thick) and sub-μm thick Nafion films[25] (Fig. 5b). In bulk Nafion membrane, proton conduction environment (assessed from I_d/I_p profile) was almost uniform across the membrane. However, proton conduction of Nafion thin films (on glass substrates) was extremely weak over a broad region next to the substrate interface, then gradually increased as we approached the air interface (Fig. 5b).[25] The overall I_d/I_p profile was found to be thickness- and humidity-dependent. However, humidification could not make the near-substrate region more favorable for proton conduction (Fig. 5b, $z/d \sim 0$). It was also interesting to see that low-proton-conducting region propagated up to about half of the Nafion films starting from the substrate interface (studied 68–1000 nm thick Nafion films).

NR measurements indicated water accumulation near the substrate interface of sub-μm thick ionomer[73–75] films; while our CLSM images suggested that ionomer chains and these water molecules

residing near the substrate interface do not conduct protons efficiently.[25] The NR-CLSM observations corroborate with the surface-parallel alignment of Nafion backbones next to substrate[61] compelling their side-chain –SO₃H to face and pin to the substrate (Fig. 5c). Such pinned ionomer chains should have lower segmental mobility. Also, the water molecules H-bonded to this substrate and substrate-pinned ionomer chains will have their rotational mobility compromised. When we looked at CCVJ-stained and hydrated Nafion films under CLSM, we identified a stiffened region next to the substrate within these Nafion films.[25] Moreover, the width of the antiplasticized region near the substrate interface was comparable to the width of the low-I_d/I_p region of a film. This demonstrated the critical role played by interfacial processes and water-ionomer mobility on thin-film ionic conductivity.

Having said that, the water-rich layers, identified by NR, are much thinner ($\sim$10 nm) than the low-conducting, low-mobility regions (about half of film thickness) captured by CLSM. This suggested that the substrate interface alone likely does not control the mobility and conductivity. We observed hump-like mobility distribution curves (CLSM) indicating the lowest mobility in the film's middle. This could be attributed to polymer chain or chain segment crowding in this region.[68] Apparently, it made sense because the mid-region of Nafion films on SiO₂ was more polymer-rich than the next-to-substrate region (NR).[77] Others reported maximum chain entanglement density in the middle of the films.[141] Dense packing of entangled polymer chains can lower the chain mobility and stiffen the mid-region of the films. Lastly, if some chains are pinned to the substrate at one end, and extend across the film, their mobility may be controlled by substrate.[142] Together these facts (Fig. 5c-right) explain the origin of broad, low-conducting, low-mobility regions in Nafion films. In contrast, the air interface, free from these constraints, showed better proton conduction.

Overall, this CLSM-based strategy made a groundbreaking advancement in our understanding of ionomer thin films and ionomer–substrate interfaces. Previously, we had no other choice but to rely on an average value of proton conductivity (σ) for an entire ionomer sample, measured using electrochemical impedance spectroscopy (EIS). Now, we can reveal the depth-specific proton conduction behavior and tell how far the interfacial effects propagate inside very thin films. After demonstrating the proof-of-concept, we extended this CLSM-based strategy to understand several ionomeric systems.[23,29,48] Especially, we used CSLM to distinguish the depth-specific proton-conduction environment across Nafion films on unmodified and engineered substrates.[29] We also located a specific feature in a film of a biomimetic ionomer and assessed proton conduction across the feature.[23]

ENGINEER ionomer–substrate interface

Can we manipulate the distribution of ion conduction environment?

Realizing that interfacial interactions are detrimental to water–polymer mobility[24,25,55,70,75,143] and proton conduction,[24,25] leading to poor proton conduction over a broad region near the substrate (Fig. 5b), we started to think if we can manipulate the interfacial makeup in a way to improve thin-film proton conductivity and alleviate ion transport limitations. Interfacial engineering is crucial for ionomer–catalyst binder layers in PEMFC cathodes, as surface-parallel ionomer chains can cover catalyst particles, block ORR active sites, cause gas (O₂) transport limitation, and reduce PEMFC performance.[32,48,132,144,145]

To date, various approaches have been employed to engineer model substrates and catalysts to alter their physical and chemical properties. Apart from altering the structure and chemistry of catalysts,[146–148] interfacial restructuring of model substrates has been grabbing attention lately. For example, substrate hydrophilicity[147,149–151] or zeta potential[147] was altered, substrate interface was doped with certain atoms[152–154] or modified *via* covalent/electrostatic immobilization of certain molecules, like, block copolymers, ionic liquids (ILs),[151,155–158] IL-modified block copolymers,[31,159,160] or peptides.[32,71,161] Different approaches impact substrates and electrodes differently. For instance, Renner *et al.*[32] modified Pt electrodes with genetically engineered peptides having Pt-binding domains. The –NH₂ groups of Pt-bound peptides enabled Nafion adsorption on Pt with altered film morphology and higher Pt-coverage. On the contrary, block copolymers with both –SO₃H and IL moieties (SPILBCPs)[31] doubled the kinetic performance of MEAs due to reduced coverage of the Pt surface. Snyder *et al.*[30] improved electrocatalyst performance inside pores of the electrodes by embedding catalysts with hydrophobic protic IL. In general, rendering hydrophobicity to surfaces[147,149–151] or favorably orienting the lamellar structure[162,163] may weaken the adsorption of –SO₃⁻ anions of Nafion chains onto the substrate.

Our hypothesis was that a porous or brush-like or spider-web-like architecture near the substrate could prevent surface-parallel alignment and anchoring of ionomers and enhance proton conduction. As proof of concept, we adopted a simple yet robust substrate engineering approach. First, we treated the substrate interfaces with (3-aminopropyl)triethoxysilane (APTES), and then deposited sub-μm thick Nafion films on top (Fig. 6a).[29] Prior endeavors in this field primarily focused on materials development. Our goal was not just to demonstrate a new interface engineering approach, but to delve into underlying mechanisms driving proton conductivity through addressing fundamental, unexplored questions. For instance, existing literature lacks interface- and depth-specific information on proton conduction which we explored using our previously established CLSM protocols.[25] This unique interface-specific information was complemented further by looking into the physical, chemical and mechanical change happening at the substrate interface.

Our investigation uncovered that APTES modification reduced the hydrophilicity of the SiO₂ substrate and boosted both in-plane (σ_{IP}) and out-of-plane (σ_{OP}) proton conductivity of Nafion thin films (Fig. 6b).[29] For example, in Nafion films with thickness ($\sim$60 nm) closer to catalyst binder ionomer layers in PEMFCs, silane induced 2-times improvement in σ_{IP} and at least 10-times improvement in σ_{OP} (Fig. 6b). APTES itself had negligible conductivity, thus had negligible contribution to the total conductivity of the Nafion-silane ensemble. Most importantly,
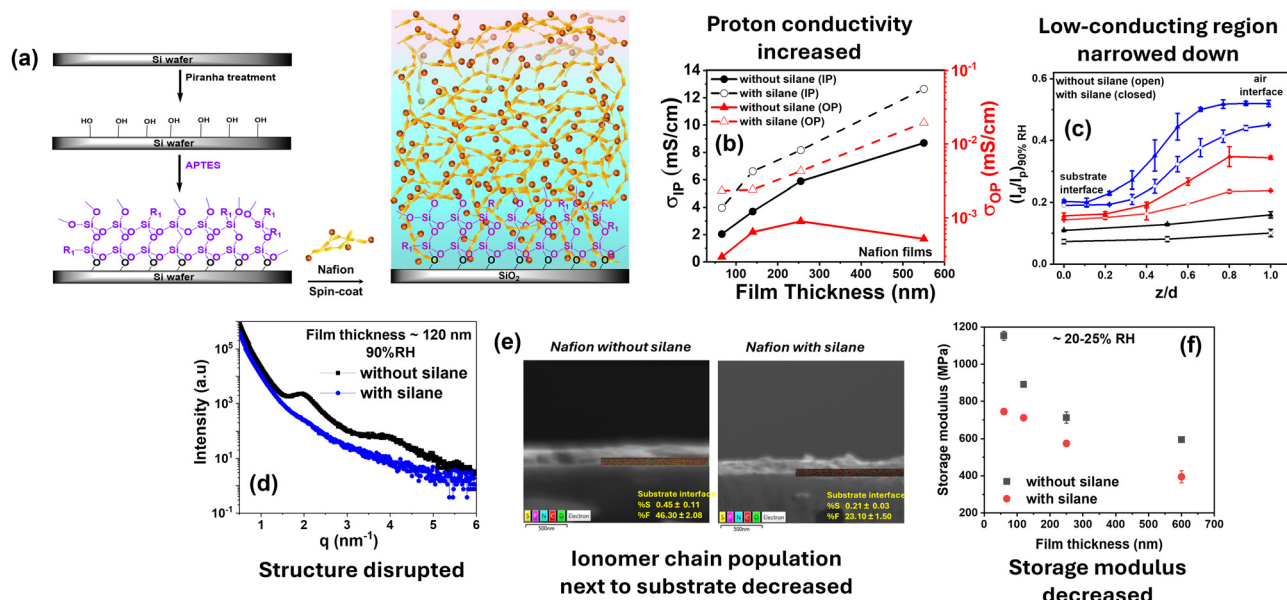
Fig. 6 (a) Schematic representation of surface engineering of SiO₂ surface using a silane linker (APTES) and subsequent preparation of Nafion thin films. (b) In-plane (σ_{IP}) and out-of-plane (σ_{OP}) proton conductivities of Nafion thin films on unmodified vs. silane-modified surfaces at ∼83–86% RH as function of film thickness.[29] (c) I_d/I_p profile of ∼250 nm thick Nafion films with silane (red) or no silane (black) underneath at 90% RH.[29] Films were stained with HPTS. (d) 0D-GISAXS profiles of ∼250 nm thick Nafion films on unmodified- and APTES-modified substrates at 90% RH.[29] (e) SEM-EDX cross-sectional images of ∼150 nm-thick Nafion films on SiO₂ (left) and APTES-SiO₂ (right) substrates showing elemental mapping at the substrate interface (boxed regions).[29] The elements S, F, N, C, and O are represented by yellow, cyan, blue, red, and green, respectively. The dimension of the boxes in which we did elemental analysis is 75 nm (height) × 1350 nm (length). (f) Storage modulus at ∼20–25% RH of 50–600 nm-thick Nafion films on untreated and silane-treated surfaces respectively.[29] Figures reprinted with permission from ref. 29. Copyright 2024, American Chemical Society.

APTES-based substrate modification narrowed down the low-conductivity region next-to-substrate and an overall enhancement in protonic conduction behavior across the entire Nafion films on silane, as revealed by I_d/I_p profile from CLSM imaging (Fig. 6c).[29]

Interestingly, silane did not alter the water uptake by the Nafion films, but significantly altered the phase segregation, ionomer chain packing, pinning, orientation, and distribution of Nafion chains.[29] The loss of correlation in Nafion films deposited on silane-modified substrates (GISAXS, Fig. 6d) manifested an induced disorder in lamella and/or a randomization of ionomer chains in all directions.[29] Moreover, SEM-EDX-based elemental mapping showed that the APTES layer over the substrate led to a reduced population of Nafion chains next to the substrate (Fig. 6e). For example, %F, %S near substrate interface of ∼150 nm thick Nafion films: 46.3%, 0.45% (no silane); 23.10%, 0.21% (with silane).[29] The APTES layer also altered ionomer chain orientation in the films overall and led to a more isotropic (randomized) chain structure. The randomization was such that it favored proton conduction more in thin Nafion films on APTES. Last but not least, silanization reduced the elastic modulus of Nafion films (Fig. 6f) indicating reduced Nafion-substrate interactions and reduced chain pinning to substrate upon silanization, making Nafion films on silane less stiff than that on unmodified substrates.[29]

Overall, this surface engineering approach[29] offered a promising pathway to alter the physical–chemical makeup of the ionomer–substrate interface, negate interfacial lamella and chain pinning, and improve interfacial as well as across-the-

film proton conductivity of Nafion. It opened new avenues to overcome the ion-transport limitation. Especially, the study provided deep mechanistic insights into interfacial phenomena and the propagation of their effects, distinguishing it as a unique contribution to the field. Combining findings from EIS, CLSM, GISAXS, SEM-EDX, ellipsometry, and CR-AFM created a comprehensive platform to understand interfacial processes in ionomer–substrate and ionomer–catalyst systems, relevant to diverse electrochemical technologies like fuel cells, electrolyzers, and batteries. Currently, our focus lies in comprehending the impact of different functionalization on interfacial ion conductivity, aiming to further optimize proton conduction in thin film systems (reported in future communications).

DESIGN new ionomers to improve thin-film and interfacial proton conductivity

Based on our current understanding, it is time to realize that for the catalyst binder layer, we should prioritize using the ionomers specifically designed keeping in mind the specific issues associated with ionomer thin films over those originally intended for membranes. This is because the design needs for ionomers for catalyst binder layers are distinctly different from those for bulk membranes. We revealed that interfacial effects, poor phase separation, and small, scattered, poorly connected
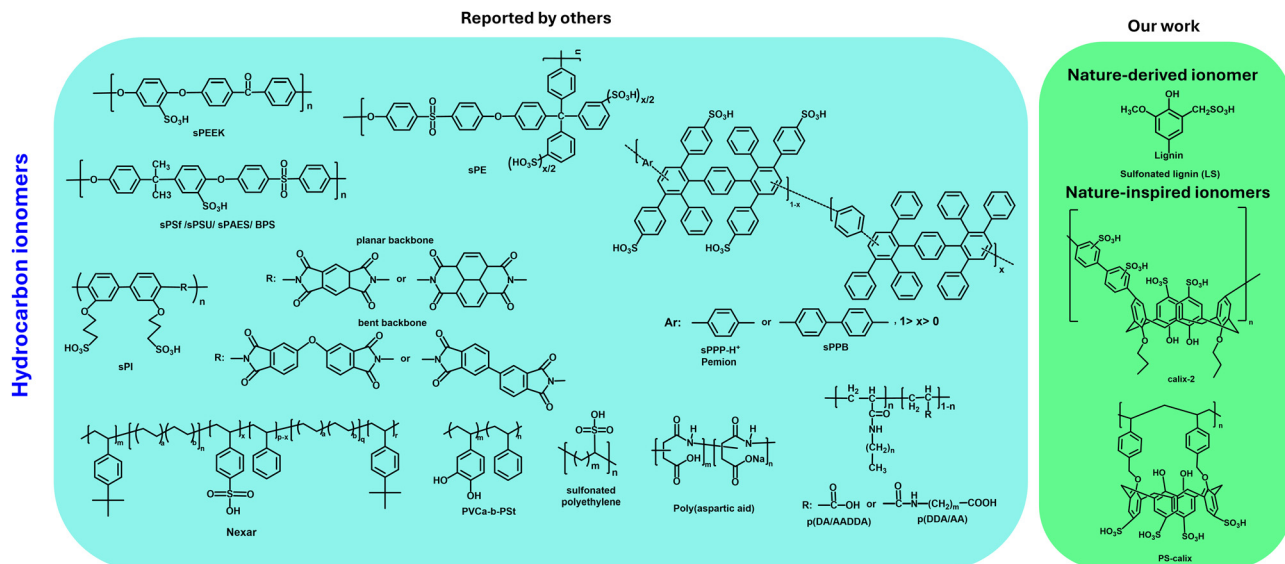
Fig. 7 Chemical structures of hydrocarbon-based ionomer classes studied in thin films or at MEA level. Chemical structures redrawn with permission from refs: sPEEK: sulfonated poly(ether ether ketone);[99] sPE/sPSf/sPSU/sPAES/BPS: derivatives of sulfonated polysulfone or poly(arylene ether sulfone);[48,109,111,166] sPPP: sulfophenylated poly(phenylene);[114] Pemion: derivative of sulfophenylated poly(phenylene);[118] sPPB: sulfophenylated poly(phenylene) biphenyl[22] Nexar: sulfonated styrene-based pentablock terpolymer;[117] p(DA/AADDA): polyethylene with acrylamide and amidoalkylcarboxylic acid side chains;[167] p(DDA/AA): polyethylene acrylamide and carboxylic acid side chains;[168] sPI: derivatives of sulfonated polyimide;[169] polypeptide;[170] PVCa-*b*-PSt: poly(vinyl catechol)-*block*-poly(styrene);[171] LS: lignin sulfonic acid;[70] calix-2: sulfonated calix[4]arene-sulfonated biphenyl;[23] PS-calix: polystyrene backbone with sulfonated calix[4]arene pendants.[48] Copyrights 2013, 2015, 2016, 2018, 2022, American Chemical Society; Copyright 2023, Cell Press; Copyright 2020, Frontiers; Copyrights 2008, 2015, 2021 Elsevier; Copyright 2001, 2018 Wiley; Copyrights 2007, 2019, 2020, The Electrochemical Society; Copyright 2021, Royal Society of Chemistry.

ionic domains[24,44,96] are the major issues adversely affecting the proton conductivity of ionomer thin films mimicking catalyst binder layers. Our observations are in complete agreement with what DOE-Hydrogen and Fuel Cell Technologies Office (DOE-HFTO)'s 2023 annual merit review[5] reported. As per the report, by advancing the ion and gas transport pathways in electrode design, up to ~50% higher power density can be achieved.[5,164] The report also suggests pathways to reduce PEMFC stack costs. By increasing power density and reducing the loading of platinum group metal (PGM) catalysts in electrodes, PEMFC system cost can be reduced by 20%.[5] The connection between proton conductivity, power density and cost is: high proton conductivity would lead to high ORR efficiency and high power density; and achieving high power output from relatively smaller PEMFC stacks would reduce stack manufacturing costs.[11]

Therefore, any ionomer that can alleviate proton transport limitation while minimizing cost and environmental concerns, would be ideal as ionomer binders for PEMFCs. The high-cost (Nafion: $500 per kg)[165] and environmental concerns of fluorocarbon-based ionomers have made the research community shift toward hydrocarbon-based ionomers. At the current context, with raised concerns about perfluorinated compounds (PFAS), this transition is even more important. However, as discussed earlier, traditional fluorocarbon (Nafion)- and hydrocarbon-based ionomers (sPSf, sPEEK), designed for membranes and conducting protons efficiently in bulk membranes, perform poorly in thin films and cathode catalyst layers or MEAs. For instance, Nafion

thin films (9 mS cm^{-1}) showed over an order of magnitude higher proton conductivity than sPSf films (0.2 mS cm^{-1}).[48] Binder-phase/MEA-level studies of traditional hydrocarbon-based ionomers (Fig. 7, left panel and Table 3) also supported severe diffusion limitations[18,19] and lower power densities.[20–22] As can be seen in Table 3, at comparable testing conditions, the power densities of MEAs made of typical hydrocarbon-based ionomers were roughly an order of magnitude lower than fluorocarbon-based ones at 0.7 V. While fluorocarbon-based MEAs exhibited a power density around 1 W cm^{-2} at 0.7 V (Table 3),[8,105] the desired power density for fuel cell vehicles is 2.1–3.2 W cm^{-2} at 0.7–0.8 V (equivalent to a current density of 3–4 A cm^{-2} at 0.7–0.8 V).[9] Catalyst design has received much attention and efforts,[10,26–28] but ionomer design for catalyst binder layers has long been overlooked. In fact, the tendency has been to employ the same ionomers as catalyst binders that work well for membranes. This is where we contributed over the last few years.

The earlier limited, thin-film focused ionomer design efforts relied majorly on creating extreme lamellar structures using polyimide,[169,172–174] polypeptide,[170,175] and polyethylene[167,168,176] derivatives (Table 4 and Fig. 7, left panel highlighted blue). The fundamental idea behind these efforts was to achieve an ordered layered structure to enable transport better than tortuous pathways. Creating highly preferential alignment of ionomer chains (lamella) gave rise to enhanced in-plane proton conductivity, but at the same time, made proton conduction highly anisotropic.[167,168,175] This is expected as the surface-parallel

Table 4 Proton conductivity of reported ionomers in thin films

Ionomer	IEC	Substrate	Annealing condition	Film thickness (nm)	%RH	Temperature (°C)	Proton conductivity[a] (mS cm^{-1})	Ref.
Polyimide backbone								
Sulfonated polyimide (linear)	2.89–3.11	SiO$_2$	Unannealed	500	95	25	158	169
Sulfonated polyimide (bent)	2.72–2.78	SiO$_2$	Unannealed	500	95	25	63	169
Sulfonated polyimide (oriented lamella)	2.9	SiO$_2$	Unannealed	500	95	25	150	172
Sulfonated polyimide (disoriented lamella)	2.9	SiO$_2$	Unannealed	500	95	25	30	172
Sulfonated polyimide-*block*-hydrophobic polyimide	2.69	SiO$_2$	Unannealed	500	95	25	32	173
Polyethylene backbone								
Acrylamide and amidoalkylcarboxylic acid side chains, p(DA/AADDA)	n.a.	Hydrophobic glass	Unannealed	900	98	60	1.7×10^{-3} (IP) 4×10^{-6} (OP)	167
Acrylamide and carboxylic acid side chains, p(DDA/AA)	n.a.	Hydrophobic glass	Unannealed	60	98	60	51 (IP) 2×10^{-11} (OP)	168
Acrylamide and vinylphosphonic acid side chains	n.a.	Hydrophobic silicon	Unannealed	—	98	60	32	177
Folded backbone with precisely positioned sulfonic acid side chain	n.a.	None (Free-standing film)	Annealed	200 000	100	40	100	176
Polypeptide backbone								
Poly(aspartic acid)/sodium aspartate	n.a.	MgO	Unannealed	60	70	25	3.4	170
Poly(aspartic acid)/sodium aspartate	n.a.	Glass	Unannealed	60	50	25	2.7×10^{-3} (IP) 3.4×10^{-6} (OP)	175
Polystyrene backbone								
Poly(vinyl catechol)-poly(styrene) block copolymer-Ag np, PVCa-*b*-St	n.a.	Quartz	Unannealed	200	95	n.a.	0.1	171
MOF								
Cu-TCPP nanosheet	n.a.	SiO$_2$	Unannealed	350	40	25	3.2×10^{-5}	178
					90		6.2×10^{-2}	
COF								
Nafion	1	SiO$_2$	Unannealed	25 000	90	30	7	120
SDT-COF-Nafion	1.70 (COF)						10.5	
Our Works								
LS	1.6	SiO$_2$ (thermal oxide	Annealed	25	85	25	4	70
				165			14	
Calix-2	3.9	SiO$_2$ (thermal oxide)	Unannealed	20	83	25	22.57 (IP) 1×10^{-5} (OP)	23
				100			65.5	
PS-calix	3.85	SiO$_2$ (thermal oxide)	Unannealed	15–20	85	25	41.1	48
				160			65.4	
sPSf	1.3	SiO$_2$ (thermal oxide)	Unannealed	15–20	85	25	0.01	48
				160			0.2	
Nafion	0.99	SiO$_2$ (thermal oxide)	Unannealed	15–20	83	25	3.3 (IP) 3×10^{-6} (OP)	48
				100			8.3	23
				160			9	48
Nafion	0.99	SiO$_2$ (thermal oxide)	Annealed	25	85	25	0.13	70
				165			1	

[a] Unless otherwise stated, proton conductivities are measured in-plane direction. The terms "IP" and "OP" represent proton conductivity at in-plane and out-of-plane directions.

lamella in Nafion thin films does the same (*e.g.*, σ: 3.3 mS cm^{-1} (IP) *vs.* 3×10^{-6} mS cm^{-1} (OP) for ~20 nm thick Nafion film, Table 4) and we showed that avoiding or disrupting near-substrate lamella may improve both in-plane and out-of-plane proton conductivity (Fig. 6b).

Our synthetic ionomer design approaches, on the contrary, concentrated more on gaining control over ionic domain size and connectivity and creating multimodal proton hopping pathways. Our ionomer design efforts so far thus can be classified into two categories (Fig. 7, right panel, highlighted green): (i) nature-derived ionomers, and (ii) nature-inspired ionomers. The nature-derived approach[70] leveraged plant polymer lignin as precursor yielding low-cost, sustainable, PFAS-free ionomers with high thin-film proton conductivity. In the nature-

inspired approach,[23,48] we got inspired by biological ion channels and brought their capabilities into the design of synthetic proton-conducting ionomers which showed proton conductivity superior to Nafion in thin films. Here, we summarily discuss the outcome of these efforts.

Nature-derived ionomers

Lignin-based ionomers conduct protons more efficiently than Nafion in thin films

Traditional hydrocarbon-based ionomers, like sPEEK or sPSf differ from fluorocarbon-based ionomers in several key aspects: they have less flexible backbones with less acidic sulfonic acid
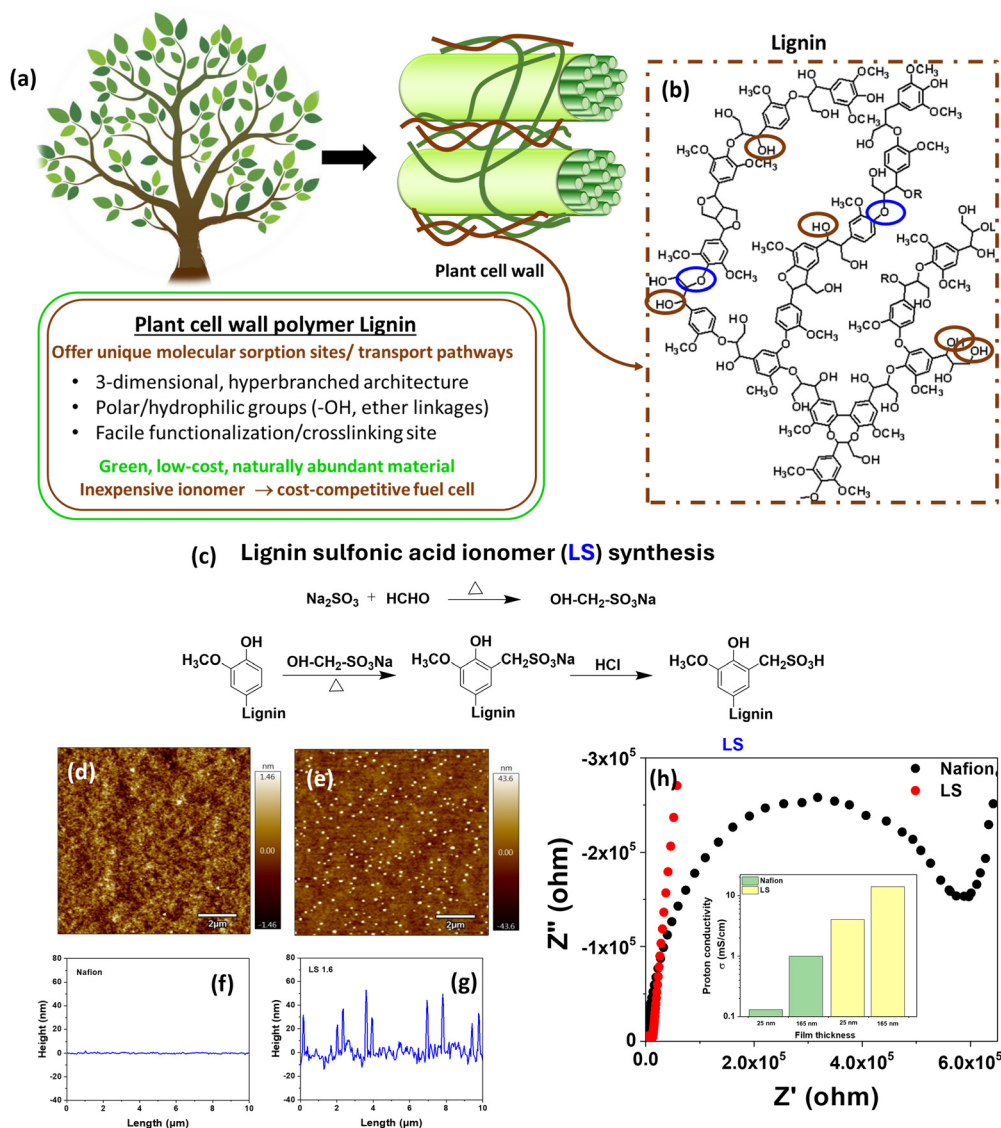
Fig. 8 (a) and (b) Features of lignin making it suitable for designing ionomers. (c) Synthetic pathway to design lignin-based ionomer (LS). (d) and (e) AFM images and (f) and (g) corresponding roughness profiles of Nafion (left) and LS (right) films. (h) Nyquist plots and (h, inset) proton conductivities of Nafion and LS thin films at 85% RH.[70] Figures adapted with permission from ref. 70. Copyright 2020 Frontiers.

groups at side chains (pK_a: −1 (–SO$_3$H) in sPEEK $vs.$ −6 (–CF$_2$–SO$_3$H) in Nafion),[122,179] less pronounced phase separation,[122,179] less free volume,[180] low density of protonic sites,[118] low protonic mobility,[122] and narrow, tortuous, and isolated ion-conducting channels.[122,179] Also, most of these linear hydrocarbon ionomers block catalytically active surface sites.[18] These features hinder proton conduction and gas transport in thin films.[14,16,18,48,103,179] We thus need new ionomer formulations to improve proton conduction in thin films, be cost-effective and environmentally friendly at the same time. This quest motivated us to explore plant cell wall polymer, lignin (Fig. 8a).

Lignin has many structural features (Fig. 8a and b) which makes it an ideal synthetic precursor of ionomers.[70] Lignin is the second most naturally abundant polymer. It is a 3-dimensional hyperbranched polymer that has plenty of polar ether (–O–) linkages and hydroxyl (–OH) groups. Within the network-like

structure of lignin, these polar/hydrophilic groups can welcome water needed to generate ion-conducting pathways. We functionalized lignin with –SO$_3$H groups to design lignin-based proton-conducting ionomers (LS, Fig. 8c). By controlling lignin-to-sulfonating agent ratio, the ion exchange capacity (IEC) was effectively controlled to achieve lignin sulfonic acid (LS) ionomers which were not water-soluble, unlike the commercial water-soluble lignosulfonate coming from pulp and paper industries. This approach enabled us to design lignin-based practical ionomers[70] which will not get washed away while conducting protons in the hydrated state in thin films.

LS formed uniform and smooth films when spin-coated. Also, LS films were less dense than Nafion or sPSf in thin films which agreed with the hollow, network-like structures that facilitated the formation of 3D, connected ion-conduction pathways.[70] AFM images showed significantly different morphology with

ellipsoidal self-assembled features in LS films (Fig. 8d–g). Also, by fitting the ionic domain peaks (GISAXS) of Nafion and LS films in geometric models (core–shell, ellipsoidal, cylindrical), we found that LS films showed much larger ionic domains as compared to Nafion films (e.g., 1.55 nm (Nafion) vs. 7.5 nm (LS)). The observation of larger ionic domains in LS films was in total agreement with the proton conductivity values. LS offered significantly higher proton conductivity than Nafion in thin films (Fig. 8h).[70] For instance, a ~25 nm thick LS film (thickness similar to ionomer binder layer) showed proton conductivity ~4 mS cm^{-1} which was more than an order of magnitude higher than a Nafion film with similar thickness (Table 4). The same order of magnitude of proton conductivity improvement was achieved for thicker LS films. Additionally, LS films, unlike Nafion films, did not stiffen upon humidification,[70] suggesting more mobility of water-ionomer inside LS films. Thus, the larger ionic domains and higher mobility facilitated increased proton conductivity of LS films. Together, the work paved a new way towards designing lignin-based, low-cost, efficient, sustainable, PFAS-free ionomers capable of circumventing the ion conduction limitation of PEMFC electrodes.

Lignin is not only abundant in forests and agricultural residues but also found as a by-product from pulp and paper industries and cellulosic biorefineries. However, only 1–2% of this lignin is valorized[181–187] and the rest is either burnt or wasted. Traditionally, lignin's use in energy materials has mostly circled around creating carbon materials for electrodes.[188–194] The 2023 Billion-Ton Report (BT23)[195] from the U.S. Department of Energy (DOE)'s Bioenergy Technologies Office highlights the need to rethink our energy systems to decarbonize the economy, emphasizing the potential of waste feedstocks and biomass. By designing lignin-based, environment-friendly solid polymer electrolytes and advancing the design of clean energy technologies, we can bring innovation in lignin valorization. Such efforts can potentially enhance the economic viability of industries (including biorefineries), and support bioeconomy and energy economy simultaneously. While source-to-source variation and limited understanding of unmodified lignin are often considered as challenges to adopt lignin in energy materials, we are up for embracing these challenges and tackling the issues. We plan to extend our studies to various lignin sources and conduct in-depth molecular-to-nanoscale characterization before materials design, aiming to create an extensive database on lignin-based materials.

Nature-inspired ionomers

In thin films of traditional ionomers, ionic domain formation is severely sacrificed as ionomers lose mobility and cannot efficiently phase separate. We looked for a workaround with a hypothesis: if we can design ionomers having hollow, cavity-forming repeat units with ion-conducting functionalities, at least molecular-level ion transport should be possible through the built-in, molecular-level pores, even when the ionomers are sitting idle and not segregating for well-formed phases. If, by any chance, these ionomers, having hollow, cavity-forming

units, can self-assemble in solution (literature supports[196–199]), and retain the assembly in the solid state in a way that stacks the pores, we will be able to achieve both short-range and long-range proton conduction pathways and improve proton conductivity in thin films.

The understanding of traditional ionomers aligns with a generalized thought, i.e., proton conductivity declines as the ionic domains shrink in size. For example, the average size of ionic domains in bulk Nafion membranes is 4 nm, while it shrinks to ~1–2 nm with poor domain connectivity in Nafion thin films. Then we also learned from the literature that there can be a striking difference in water-ion transport mechanism when the size of ionic domains/ion channels transitions from narrow (>1 nm) to very narrow (<1 nm).[200,201] Biological ion channels are very narrow (<1 nm), but they can transport water and/or ions very efficiently. For example, Gramicidin A[202] has a sub-nm pore diameter (~4 Å), but it transports protons very fast. Explaining the proton-conduction mechanism across such very narrow pores is still a work in progress,[203–211] but a mechanism that is often put forward is: water in sub-nm sized channels with hydrophobic interiors experience frictionless slip flow[212] allowing water to diffuse even faster than bulk water. The underlying principle is that unlike branched, H-bonded, 3D water networks in bulk water, water passing through sub-nm pores or channels is compelled to form 1D water wires,[209,210] where water dipoles are preferentially oriented to facilitate proton hopping.[209–211] Also, the mobility-retarding effects of H-bonding are alleviated due to the hydrophobic interior of the pores.

A range of porous materials has been reported with broad range of pore size, including polymers with intrinsic microporosity (PIMs),[213] metal–organic framework (MOF),[214] covalent organic framework (COF),[120,215] imidazole quartets,[216] triazole channels,[217] graphene,[218,219] cyclic peptide nanotubes,[220] carbon nanotubes (CNTs)[200,211,221] and electrospun hollow nanofibers.[222] A large faction of these materials primarily targeted to study host–guest interactions, sensing, gas adsorption, water purification, separation, and osmotic power-driven energy systems.[196,207,223–230] Some targeted to improve proton conductivity (e.g., PIM, MOF, COF), but majorly aimed for bulk membranes.[222,231,232] Many of these are crystalline and/or insoluble giving rise to solution/thin-film processability and stability issues.[233,234] The innovation lies in the design of ionomers having sub-nm-sized hollow repeat units[235] – something the community designing fuel cell/battery ionomers has not been considering. Summarily, for thin films/catalyst layers, there remains a need for porous solid conductor showing a combination of precise angstrom-scale pores, good processability,[214,236] compatibility with catalyst ink materials,[214] and elevated proton conductivity in sub-μm thick films and interfaces – critical yet rarely addressed issue in PEMFCs and other electrochemical devices.[70,237] To address these needs, we brought the capabilities of biological ion channels into the design of proton-conducting ionomers to enhance proton conductivity under thin film confinement.

Macrocycles can enable thin-film proton conductivity much higher than Nafion

To mimic biological ion channels, we leveraged the molecular features of calix[4]arene, a hollow and extremely narrow
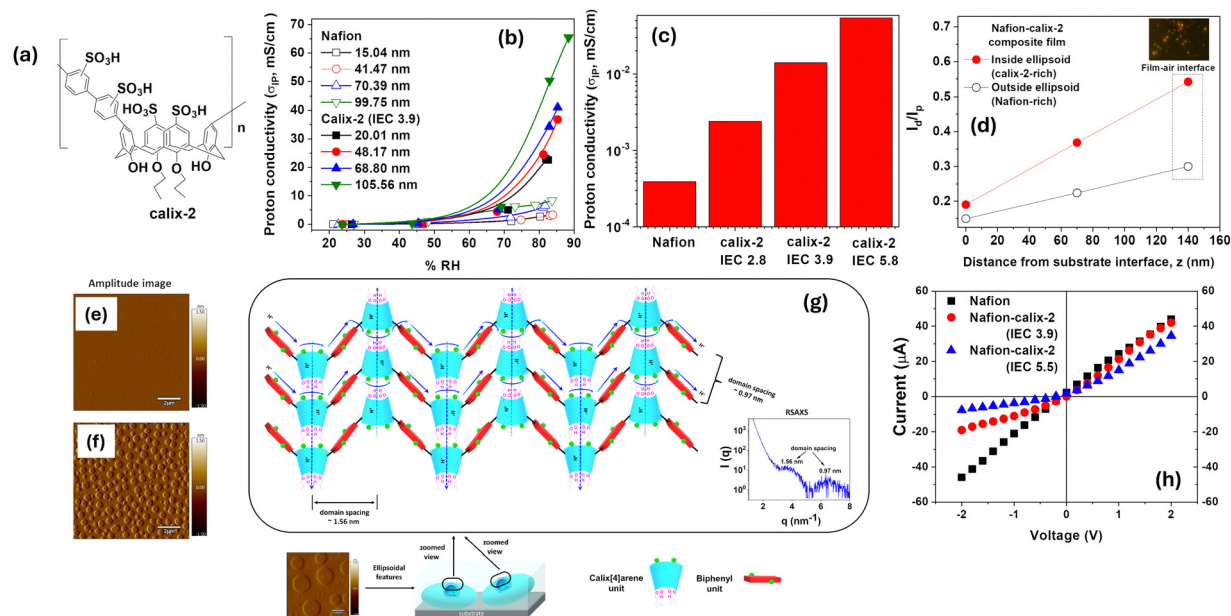
Fig. 9 (a) Chemical structure of calix-2 ionomer. (b) In-plane proton conductivity (σ_{IP}) of Nafion and calix-2 (IEC = 3.9) films with different thicknesses as a function of % RH. (c) In-plane proton conductivity (σ_{IP}) of ~15 nm thick Nafion and calix-2 films at 20–25% RH. (d) and (e) AFM amplitude images of ~35 nm thick films of Nafion (d) and calix-2 with IEC 3.9 (e). The scale bars shown within the images were 2 μm. (f) Proposed self-assembly modes and ionic conduction pathways within calix-2 ionomer films based on AFM and GISAXS data. ((f), inset, right) GISAXS pattern of calix-2 (IEC 3.9) film at 92% RH. The solid blue arrows represent surface proton hopping, while the dotted blue arrows represent the proton conduction across individual macrocyclic cavities as well as self-assembled ion channels through multiple cavities. The green balls attached to calix[4]arene (blue) and biphenyl (red) units represent sulfonic acid (−SO₃H) groups. (g) Through-plane proton conduction (I_d/I_p) profile of a Nafion-calix-2 composite film (~140 nm thick) at 80% RH. The inset shows the CLSM image of the film at the film-air interface (scale bar 1 μm). The I_d/I_p values at this film-air interface are shown within the dotted black box. Here the IEC of the calix-2 used to make the film was 3.9. (h) I−V curves of Nafion and Nafion-calix-2 (IEC 3.9, IEC 5.8) composite membranes were recorded in 0.1 M KCl in DI water. Figures reproduced with permission from ref. 23. Copyright 2022, American Chemical Society.

macrocycle (~3 Å). In our first effort in this direction, we designed an ionomer, calix-2 (Fig. 9a), having sulfonated calix[4]arene and sulfonated biphenyl repeat units.[23] Calix-2 forms uniform thin films which address the processibility issue. In ≤100 nm thick films, in-plane proton conductivity of calix-2 (65.5 mS cm⁻¹) was up to 8 times higher than the current benchmark ionomer Nafion at 85%RH (Fig. 9b), and over an order of magnitude higher than Nafion at 20–25% RH (Fig. 9c). This highlighted the significant improvement in proton conductivity achievable with macrocyclic repeat units. Not only that, but we also saw a significant improvement of both in-plane and out-of-plane proton conductivity when calix-2 was used. For instance, for 20 nm thick unannealed films, the proton conductivities were as follows: Nafion: σ_{IP}: 3.3 mS cm⁻¹, σ_{OP}: 3 × 10⁻⁶ mS cm⁻¹ *vs.* calix-2: σ_{IP}: 22.6 mS cm⁻¹, σ_{OP}: 1 × 10⁻⁵ mS cm⁻¹ (Table 4). The reduced anisotropy in proton conductivity and improved out-of-plane proton conductivity (in addition to in-plane) was uniquely different from extreme lamella-forming ionomers (Table 4).

Proton conduction is better at places where macrocycles are located

To further validate the role of macrocycles, we synthesized a non-macrocyclic ionomer with only sulfonated biphenyl units (SBP). Calix-2 showed about 5-orders of magnitude higher proton conductivity as compared to this non-macrocyclic

variant (SBP). For instance, a 49 nm thick SBP film at 80% RH exhibited proton conductivity of 7 × 10⁻⁴ mS cm⁻¹, while it was 37 mS cm⁻¹ for calix-2.[23] Additionally, a composite film of SBP and monomeric sulfonated calix[4]arene (Scalixmono) in a 1:0.2 wt ratio showed proton conductivity of 17.5 mS cm⁻¹, significantly higher than pure SBP.[23] Furthermore, incorporating the photoacid dye HPTS in Nafion-calix-2 composite films demonstrated that proton conduction was stronger at places where macrocycles were located and weaker where Nafion was located (Fig. 9d). This array of evidence reinforced the role of hollow macrocyclic cavities in enhancing thin-film proton conductivity.

Macrocycle-based ionomers can generate multi-length scale ion-conduction pathways

While Nafion thin films appeared almost featureless (Fig. 9d), calix-2 ionomers formed ellipsoidal self-assembled structures based on amplitude and 3-dimensional AFM images (Fig. 9e). GISAXS showed two ionic domain peaks the *d*-spacing of which suggested: (i) ionic domains through macrocyclic calix repeat units; (ii) interstitial ionic pathways between two layers of single calix chains. The computed characteristic distances/dimensions from atomistic simulation closely matched with the experimentally measured domain spacing using GISAXS, suggesting that the calix units in these spherical features stacked like buckets (Fig. 9f).[23] Additionally, during DFT
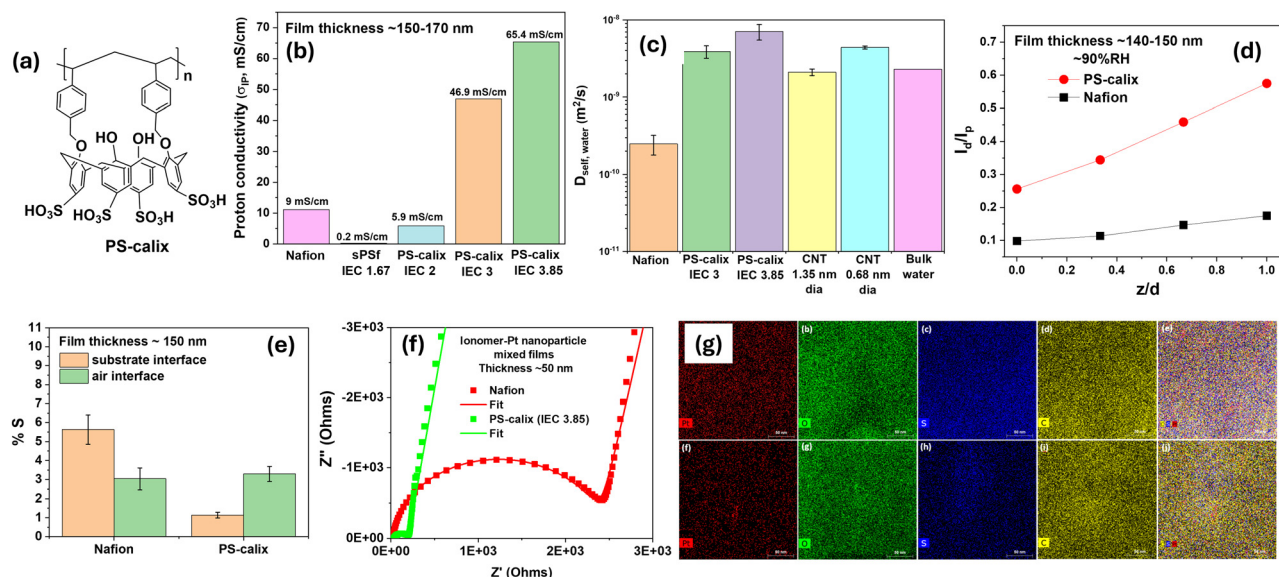
Fig. 10 (a) Chemical structure of PS-calix. (b) In-plane proton conductivity (σ_{IP}) of 150−170 nm thick Nafion, sPSf and PS-calix films at 85% RH. (c) Water self-diffusion coefficients ($D_{self,H2O}$) of Nafion, PS-calix (IEC 3, 3.85), CNTs with >1 nm and sub-nm diameters, and bulk water. Nafion and PS-calix data were obtained by us for ~300 nm-thick films at 100% RH using DOSY-NMR, while bulk water and CNT data were taken from literature for comparison.[221,238–241] (d) Proton conduction profile (I_d/I_p) across (a) ~140-150 nm thick PS-calix (IEC 3.85) and Nafion films measured using CLSM. The term z/d represents thickness-normalized distance within a film starting from the substrate interface. z/d of 0 and 1 signifies substrate and air interfaces, respectively. (e) %S at substrate and air interfaces of ~150 nm thick Nafion and PS-calix films obtained *via* elemental mapping using SEM/EDX. (f) Impedance spectra of mixed thin films containing Nafion or PS-calix with Pt nanoparticles at 85% RH. The film thickness was ~50 nm, while the diameter of Pt nanoparticles was ~3 nm. The ionomer-to-Pt mass ratio in the mixed suspension used to make the films was 10 : 0.013. (g) TEM/EDX elemental maps (Pt, O, S, C, and overlay) of ~50 nm thick PS-calix (IEC 3.85, top panel) and Nafion films (bottom panel) in which Pt nanoparticles were dispersed. The scale bar was 50 nm. Figures reprinted with permission from ref. 48, Copyright 2023, Cell Press.

optimization, we observed spontaneous proton transfer from –SO$_3$H groups to H$_2$O molecules within the channels, forming H$_3$O$^+$. Thus, stacking likely facilitated the formation of water wires inside calix channels (Fig. 9f). Consequently, proton conduction pathways in calix-2 were likely multi-dimensional: one through the calix cavities, and another along the –SO$_3$H groups on the surface of the calix repeat units.

Calix-2 ionomers did not only exhibit higher proton conductivity over Nafion in thin films and membranes, but also introduced voltage-dependent directionality in ionic current (Fig. 9h) within Nafion–calix-2 composite membranes.[23] This behavior, due to asymmetric charge distribution in calix units, resembles ionic diodes or voltage-responsive gates, a feature not present in Nafion. This allows for controlled direction and selectivity of ion transport, making these ionomers useful in various electric field-driven energy and separation applications.

Macrocycle-based ionomers can enhance both water and proton transport in thin films

In another work,[48] we synthesized a polystyrene backbone-based ionomer with sulfonated calix[4]arene as pendants (PS-calix, Fig. 10a). In films with thicknesses comparable to ionomer-based binder layers (~15–20 nm), PS-calix (IEC 3.85) exhibited conductivity (41 mS cm^{-1}) more than an order of magnitude higher than Nafion (3.3 mS cm^{-1}) and over 3 orders of magnitude higher than sPSf (0.01 mS cm^{-1}) at 85% RH (Fig. 10b and Table 4).[48] The exceedingly high proton conductivity over Nafion

was attributed to an order of magnitude faster water diffusion across PS-calix films, as measured using diffusion-ordered nuclear magnetic resonance spectroscopy (DOSY-NMR): Self-diffusion coefficient of water, $D_{self,water}$: 5×10^{-10} m^2 s^{-1} (Nafion) *vs.* 7.1×10^{-9} m^2 s^{-1} (PS-calix, IEC 3.85) at 100% RH in ~300 nm thick films (Fig. 10c). Moreover, in some cases, $D_{self,water}$ in PS-calix films exceeded the reported $D_{self,water}$ for bulk water (2.3×10^{-9} m^2 s^{-1}).[238–241] This finding aligns with the one by Noy *et al.*[221] on porous carbon nanotubes, which showed that "faster-than-bulk" water transport behavior can be achieved when the CNT diameters are reduced to sub-nm values (Fig. 10c). At these dimensions, angstrom-scale conduits can force water molecules to align into a single-file arrangement (1D water wire), allowing frictionless "slip" flow through their hydrophobic cores. Consequently, the faster-than-bulk water transport in thin films likely results from 1D water wires traversing macrocyclic cavities, a feature missing in Nafion. The concurrent observation of high water self-diffusion ($D_{self,water}$) and high proton conductivity (σ) in PS-calix indicated that macrocycle-containing ionomers can establish unique and more efficient water and ion-transport pathways, supporting our previous findings for calix-2.[23]

Macrocycle-based ionomers can minimize substrate pinning and boost thin-film proton conduction behavior

Using CLSM and photoacid dye HPTS, we demonstrated that proton conduction (I_d/I_p) at the substrate interface and across

the film significantly improved when Nafion was replaced by PS-calix (Fig. 10d). This is a unique observation as Nafion, unlike PS-calix showed a weaker proton conduction immediate next to the substrate interface (also shown in Fig. 6). Later, we also performed elemental mapping at different interfaces of ionomer films using SEM-EDX (Fig. 10e). The elemental mapping indicated that %S next to the substrate interface in PS-calix films was less than that in Nafion films. Together the observations using CLSM and SEM-EDX suggested that PS-calix chains were likely oriented in a manner reducing –SO$_3$H groups next to the substrate interface (i.e., less %S next to the substrate as compared to Nafion, Fig. 10e). Lower –SO$_3$H accumulation can reduce substrate pinning of ionomer chains, weaken substrate-induced confinement, and thus enhance proton conduction at the substrate interface (Fig. 10d) as well as across the entire PS-calix films (Fig. 10b and d) as we observed.

Macrocycle-based ionomers can address both ion- and gas-transport limitations

We noted a similar enhancement in proton conductivity when PS-calix was interfaced with Pt nanoparticles, highlighting its potential for PEMFC catalyst inks. In mixed films with Pt nanoparticles, PS-calix exhibited proton conductivity an order of magnitude higher than Nafion-Pt films (Fig. 10f). On another note, strong adsorption of ionomer chains on catalyst particles can obstruct active sites, leading to O$_2$ transport resistance in PEMFC cathodes.[59,132] We observed that PS-calix masked the Pt nanoparticles less than Nafion (Fig. 10g). By keeping more electrochemically active surface area of catalysts exposed, PS-calix can potentially reduce gas transport limitation while also alleviating ion transport limitation. These improvements in both ion- and gas transport properties at nano thin catalyst interfaces using PS-calix opened new pathways for advancing ionomer design for PEMFC electrodes. By effectively channeling water and ions through appropriately sized constrictions, these PFAS-free ionomers could serve as highly efficient catalyst binder ionomer layers for fuel cells, electrolyzers, batteries, and various other sustainable energy technologies.

Broader impact, outlook, and conclusion

In this feature article, we highlighted our contribution to advancing the field of ionomers in sub-μm thick films, a relatively less explored area, but highly relevant to electrodes of clean energy technologies. Our focus was on proton-conducting ionomers relevant to PEMFCs. We developed an extensive platform to deeply understand interfacial processes and find the routes to ion transport limitations in thin films of traditional ionomers. The gained insights guided the hypothesis of engineering ionomer–catalyst interface to manipulate interfacial chemical and orientational makeup. We showed that modifying interfacial chemistry can significantly alleviate the confining effects on ionomer thin films and water molecules.[29] Finally, ionomers are rarely designed considering the factors

impeding proton conduction in nano-thin ionomer binder layers. We pioneered the design of novel fluorine-free ionomers[23,48,70] with the capability to address ion and gas transport limitations, key challenges of PEMFCs, while addressing sustainability and environmental concerns. This much-needed synthetic improvement of ionomers can transform PEMFCs and beyond.

Looking ahead, the "unraveling-engineering" efforts set the stage for exploring more complex interfacial systems in future. The systems could be ionomers at real catalyst interfaces for batteries and PEMFCs to address ion transport resistance. Also, the designed tools and strategies could be vital to understand the polymer-microbe interface to deal with antibiotic resistance, another area where we actively work on.[182,242,243] We will concurrently pursue meticulous surface nanostructuring to engineer the ionomer–catalyst interface, aiming to optimize proton and gas transport efficiency for enhanced fuel cell performance. Last but not least, while the development of novel fluorine-free ionomers surpassing traditional Nafion in performance represents a significant achievement, further research into environmentally benign synthetic pathways for these materials, understanding the stability or durability of newly designed ionomeric materials, integrating them in MEAs, and studying their performance under PEMFC-relevant conditions will further demonstrate their utility in practical device settings. Additionally, extending the applications of these new ionomers to other electrochemical and blue energy harvesting systems is a prudent and strategic progression of our work toward a sustainable, low-carbon energy future.

Data availability

This feature article did not include any primary research result, software, or code, and no new data were generated or analyzed.

Conflicts of interest

The authors declare no conflict of interest.

Acknowledgements

Notes and references

1 *Roadmap to U.S. Hydrogen Economy*, https://www.energy.gov/sites/prod/files/2017/11/f46/FCTT_Roadmap_Nov_2017_FINAL.pdf.

2 D. A. Cullen, K. C. Neyerlin, R. K. Ahluwalia, R. Mukundan, K. L. More, R. L. Borup, A. Z. Weber, D. J. Myers and A. Kusoglu, New Roads and Challenges for Fuel Cells in Heavy-Duty Transportation, *Nat. Energy*, 2021, **6**, 462–474, DOI: 10.1038/s41560-021-00775-z.

3 S. Satyapal, U.S. DOE Hydrogen and Fuel Cell Technologies Office Multi-Year Program Plan, https://www.energy.gov/sites/default/files/2024-05/hfto-mypp-2024.pdf.

4 J. Huya-kouadio and B. D. James, *Fuel Cell Cost and Performance Analysis-2023 Annual Merit Review and Peer Evaluation Meeting*, https://www.hydrogen.energy.gov/docs/hydrogenprogramlibraries/pdfs/review23/fc353_james_2023_o-pdf.pdf.

5 D. Papageorgopoulos, *Fuel Cell Technologies Overview: The Hydrogen and Fuel Cell Technologies Office (HFTO) 2023 Annual Merit Review*, https://www.hydrogen.energy.gov/docs/hydrogenprogramlibraries/pdfs/review23/fc000_papageorgopoulos_2023_o.pdf.

6 M. N. Islam, A. B. M. Basha, V. O. Kollath, A. P. Soleymani, J. Jankovic and K. Karan, Designing Fuel Cell Catalyst Support for Superior Catalytic Activity and Low Mass-Transport Resistance, *Nat. Commun.*, 2022, **13**, 1–11, DOI: 10.1038/s41467-022-33892-8.

7 N. Ramaswamy, B. Zulevi, G. Mccool, N. Patton, Z. Shi, A. Chavez, D. A. Muller, A. Kongkanand and S. Kumaraguru, Engineered Catalyst Support with Improved Durability at Higher Weight Percentage of Platinum, *J. Electrochem. Soc.*, 2023, **170**, 1–14, DOI: 10.1149/1945-7111/ad0668.

8 A. Kongkanand and M. F. Mathias, The Priority and Challenge of High-Power Performance of Low-Platinum Proton-Exchange Membrane Fuel Cells, *J. Phys. Chem. Lett.*, 2016, **7**, 1127–1137, DOI: 10.1021/acs.jpclett.6b00216.

9 K. Jiao, J. Xuan, Q. Du, Z. Bao, B. Xie, B. Wang, Y. Zhao, L. Fan, H. Wang, Z. Hou, S. Huo, N. P. Brandon, Y. Yin and M. D. Guiver, Designing the next Generation of Proton-Exchange Membrane Fuel Cells, *Nature*, 2021, **595**, 361–369, DOI: 10.1038/s41586-021-03482-7.

10 H. Wang, R. Wang, S. Sui, T. Sun, Y. Yan and S. Du, Cathode Design for Proton Exchange Membrane Fuel Cells in Automotive Applications, *Automot. Innov.*, 2021, **4**, 144–164, DOI: 10.1007/s42154-021-00148-y.

11 C. S. Gittleman, A. Kongkanand, D. Masten and W. Gu, Materials Research and Development Focus Areas for Low Cost Automotive Proton-Exchange Membrane Fuel Cells, *Curr. Opin. Electrochem.*, 2019, **18**, 81–89, DOI: 10.1016/j.coelec.2019.10.009.

12 E. Padgett and G. Kleen, *DOE Hydrogen and Fuel Cells Program Record, Title: Automotive Fuel Cell Targets and Status*, https://www.hydrogen.energy.gov/docs/hydrogenprogramlibraries/pdfs/20005-automotive-fuel-cell-targets-status.pdf? Status = Master.

13 K. More, J. Bentley and K. Reeves, Identifying Degradation Phenomena in PEM Fuel Cell MEAs Via Electron Microscopy, *ECS Transac.*, 2006, **3**, 717–733, DOI: 10.1149/ma2006-02/8/637.

14 A. Kusoglu and A. Z. Weber, New Insights into Perfluorinated Sulfonic-Acid Ionomers, *Chem. Rev.*, 2017, **117**, 987–1104, DOI: 10.1021/acs.chemrev.6b00159.

15 U. N. Shrivastava, H. Fritzsche and K. Karan, Interfacial and Bulk Water in Ultrathin Films of Nafion, 3M PFSA, and 3M PFIA

16 Ionomers on a Polycrystalline Platinum Surface, *Macromolecules*, 2018, **51**, 9839–9849, DOI: 10.1021/acs.macromol.8b01240.

16 S. Holdcroft, Fuel Cell Catalyst Layers: A Polymer Science Perspective, *Chem. Mater.*, 2014, **26**, 381–393, DOI: 10.1021/cm401445h.

17 K. Karan, Interesting Facets of Surface, Interfacial, and Bulk Characteristics of Perfluorinated Ionomer Films, *Langmuir*, 2019, **35**, 13489–13520, DOI: 10.1021/acs.langmuir.8b03721.

18 J. Peron, Z. Shi and S. Holdcroft, Hydrocarbon Proton Conducting Polymers for Fuel Cell Catalyst Layers, *Energy Environ. Sci.*, 2011, **4**, 1575–1591, DOI: 10.1039/c0ee00638f.

19 S. Sambandam and V. Ramani, Influence of Binder Properties on Kinetic and Transport Processes in Polymer Electrolyte Fuel Cell Electrodes, *Phys. Chem. Chem. Phys.*, 2010, **12**, 6140–6149, DOI: 10.1039/b921916a.

20 H. Nguyen, C. Klose, L. Metzler, S. Vierrath and M. Breitwieser, Fully Hydrocarbon Membrane Electrode Assemblies for Proton Exchange Membrane Fuel Cells and Electrolyzers: An Engineering Perspective, *Adv. Energy Mater.*, 2022, **12**, 1–19, DOI: 10.1002/aenm.202103559.

21 S. Sambandam and V. Ramani, Effect of Cathode Binder IEC on Kinetic and Transport Losses in All-SPEEK MEAs, *Electrochim. Acta*, 2008, **53**, 6328–6336, DOI: 10.1016/j.electacta.2008.04.012.

22 E. Balogun, M. Adamski and S. Holdcroft, Non-Fluorous, Hydrocarbon PEMFCs, Generating > 1 W Cm^{-2} Power, *J. Electrochem.*, 2020, **167**, 1–4, DOI: 10.1149/1945-7111/ab88bd.

23 S. Chatterjee, E. Zamani, S. Farzin, I. Evazzade, O. A. Obewhere, T. Johnson, V. Alexandrov and S. K. Dishari, Molecular-Level Control Over Ionic Conduction and Ionic Current Direction by Designing Macrocycle-Based Ionomers, *JACS Au*, 2022, **2**, 1144–1159, DOI: 10.1021/jacsau.2c00143.

24 S. K. Dishari and M. A. Hickner, Confinement and Proton Transfer in Nafion Thin Films, *Macromolecules*, 2013, **46**, 413–421, DOI: 10.1021/ma3011137.

25 S. Farzin, E. Zamani and S. K. Dishari, Unraveling Depth-Specific Ionic Conduction and Stiffness Behavior across Ionomer Thin Films and Bulk Membranes, *ACS Macro Lett.*, 2021, **10**, 791–798, DOI: 10.1021/acsmacrolett.1c00110.

26 V. R. Stamenkovic, B. Fowler, B. S. Mun, G. Wang, P. N. Ross, C. A. Lucas and N. M. Markovic, Improved Oxygen Reduction Activity on Pt3Ni(111) via Increased Surface Site Availability, *Science*, 2007, **315**, 493–497, DOI: 10.1126/science.1135941.

27 D. Li, H. Lv, Y. Kang, N. M. Markovic and V. R. Stamenkovic, Progress in the Development of Oxygen Reduction Reaction Catalysts for Low-Temperature Fuel Cells, *Ann. Rev. Chem. Biomol. Eng.*, 2016, **7**, 509–532, DOI: 10.1146/annurev-chembioeng-080615-034526.

28 G. Wu, K. L. More, C. M. Johnston and P. Zelenay, High-Performance Electrocatalysts for Oxygen Reduction Derived from Polyaniline, Iron, and Cobalt, *Science*, 2011, **332**, 443–447, DOI: 10.1126/science.1200832.

29 O. A. Obewhere and S. K. Dishari, Engineering Ionomer-Substrate Interface to Improve Thin-Film Proton Conductivity in Proton Exchange Membrane Fuel Cells, *ACS Appl. Polym. Mater.*, 2024, **6**, 4535–4546, DOI: 10.1021/acsapm.3c03218.

30 J. Snyder, T. Fujita, M. W. Chen and J. Erlebacher, Oxygen Reduction in Nanoporous Metal-Ionic Liquid Composite Electrocatalysts, *Nat. Mater.*, 2010, **9**, 904–907, DOI: 10.1038/nmat2878.

31 Y. Li, T. V. Cleve, R. Sun, R. Gawas, G. Wang, M. Tang, Y. A. Elabd, J. Snyder and K. C. Neyerlin, Modifying the Electrocatalyst − Ionomer Interface via Sulfonated Poly(Ionic Liquid) Block Copolymers to Enable High- Performance Polymer Electrolyte Fuel Cells, *ACS Energy Lett.*, 2020, **5**, 1726–1731, DOI: 10.1021/acsenergylett.0c00532.

32 N. Pramounmat, C. N. Loney, C. Kim, L. Wiles, K. E. Ayers, A. Kusoglu and J. N. Renner, Controlling the Distribution of Perfluorinated Sulfonic Acid Ionomer with Elastin-like Polypeptide, *ACS Appl. Mater. Interfaces*, 2019, **11**, 43649–43658, DOI: 10.1021/acsami.9b11160.

33 Y. Nagao, Proton Transport Property of Nafion Thin Films on MgO(100) with Anisotropic Molecular Structure, *e-J. Surf. Sci. Nanotechnol.*, 2012, **10**, 114–116, DOI: 10.1380/ejssnt.2012.114.

34 Y. Ono and Y. Nagao, Interfacial Structure and Proton Conductivity of Nafion at the Pt-Deposited Surface, *Langmuir*, 2016, **32**, 352–358, DOI: 10.1021/acs.langmuir.5b02623.

35 N. Asano, M. Aoki, S. Suzuki, K. Miyatake, H. Uchida and M. Watanabe, Aliphatic/Aromatic Polyimide Ionomers as a Proton

Conductive Membrane for Fuel Cell Applications, *J. Am. Chem. Soc.*, 2006, **128**, 1762–1769, DOI: **10.1021/ja0571491**.

36 M. Adamski, N. Peressin and S. Holdcroft, On the Evolution of Sulfonated Polyphenylenes as Proton Exchange Membranes for Fuel Cells, *Mater. Adv.*, 2021, **2**, 4966–5005, DOI: **10.1039/d1ma00511a**.

37 Y. Chang, A. D. Mohanty, S. B. Smedley, K. Abu-Hakmeh, Y. H. Lee, J. E. Morgan, M. A. Hickner, S. S. Jang, C. Y. Ryu and C. Bae, Effect of Superacidic Side Chain Structures on High Conductivity Aromatic Polymer Fuel Cell Membranes, *Macromolecules*, 2015, **48**, 7117–7126, DOI: **10.1021/acs.macromol.5b01739**.

38 Y. A. Elabd and M. A. Hickner, Block Copolymers for Fuel Cells, *Macromolecules*, 2011, **44**, 1–11, DOI: **10.1021/ma101247c**.

39 M. Yandrasits, M. Lindell, M. Schaberg and M. Kurkowski, Increasing Fuel Cell Efficiency by Using Ultra-Low Equivalent Weight Ionomers, *Electrochem. Soc. Interface*, 2017, **26**, 49–53, DOI: **10.1149/2.F05171if**.

40 M. A. Hickner and B. S. Pivovar, The Chemical and Structural Nature of Proton Exchange Membrane Fuel Cell Properties, *Fuel Cells*, 2005, **5**, 213–229, DOI: **10.1002/fuce.200400064**.

41 M. A. Hickner, H. Ghassemi, Y. S. Kim, B. R. Einsla and J. E. McGrath, Alternative Polymer Systems for Proton Exchange Membranes (PEMs, *Chem. Soc. Rev.*, 2004, **104**, 4587–4611, DOI: **10.1021/cr020711a**.

42 Z. Siroma, R. Kakitsubo, N. Fujiwara, T. Ioroi, S. Yamazaki and K. Yasuda, Depression of Proton Conductivity in Recast Nafion® Film Measured on Flat Substrate, *J. Power Sources*, 2009, **189**, 994–998, DOI: **10.1016/j.jpowsour.2008.12.141**.

43 D. K. Paul, A. Fraser and K. Karan, Towards the Understanding of Proton Conduction Mechanism in PEMFC Catalyst Layer: Conductivity of Adsorbed Nafion Films, *Electrochem. Commun.*, 2011, **13**, 774–777, DOI: **10.1016/j.elecom.2011.04.022**.

44 S. Farzin, A. Sarella, M. A. Yandrasits and S. K. Dishari, Fluorocarbon-Based Ionomers with Single Acid and Multiacid Side Chains at Nanothin Interfaces, *J. Phys. Chem. C*, 2019, **123**, 30871–30884, DOI: **10.1021/acs.jpcc.9b10015**.

45 D. K. Paul, R. McCreery and K. Karan, Proton Transport Property in Supported Nafion Nanothin Films by Electrochemical Impedance Spectroscopy, *J. Electrochem. Soc.*, 2014, **161**, F1395–F1402, DOI: **10.1149/2.0571414jes**.

46 S. Slade, S. A. Campbell, T. R. Ralph and F. C. Walsh, Ionic Conductivity of an Extruded Nafion 1100 EW Series of Membranes, *J. Electrochem. Soc.*, 2002, **149**, A1556–A1564, DOI: **10.1149/1.1517281**.

47 M. A. Modestino, D. K. Paul, S. Dishari, S. A. Petrina, F. I. Allen, M. A. Hickner, K. Karan, R. A. Segalman and A. Z. Weber, Self-Assembly and Transport Limitations in Confined Nafion Films, *Macromolecules*, 2013, **46**, 867–873, DOI: **10.1021/ma301999a**.

48 S. Chatterjee, O. A. Obewhere, E. Zamani, R. Keloth, S. Farzin, M. D. Morton, A. Sarella and S. K. Dishari, Advancing Ionomer Design to Boost Interfacial and Thin-Film Proton Conductivity via Styrene-Calix[4]Arene-Based Ionomers, *Cell Rep. Phys. Sci.*, 2023, **4**, 1–39, DOI: **10.1016/j.xcrp.2023.101282**.

49 H. Eskandari, D. K. Paul, A. P. Young and K. Karan, Humidity-Dependent Hydration and Proton Conductivity of PFSA Ionomer Thin Films at Fuel-Cell-Relevant Temperatures: Effect of Ionomer Equivalent Weight and Side-Chain Characteristics, *ACS Appl. Mater. Interfaces*, 2022, **14**, 50762–50772, DOI: **10.1021/acsami.2c12667**.

50 D. K. Paul and K. Karan, Conductivity and Wettability Changes of Ultrathin Nafion Films Subjected to Thermal Annealing and Liquid Water Exposure, *J. Phys. Chem. C*, 2014, **118**, 1828–1835, DOI: **10.1021/jp410510x**.

51 M. R. Smyda and S. C. Harvey, The Entropic Cost of Polymer Confinement, *J. Phys. Chem. B*, 2013, **116**, 10928–10934, DOI: **10.1021/jp302807r**.

52 Y. Chen, Y. Lin, J. Chang and P. Lin, Dynamics and Conformation of Semi Flexible Polymers in Strong Quasi-1D and -2D Confinement, *Macromolecules*, 2014, **47**, 1199–1205, DOI: **10.1021/ma401923t**.

53 D. Chaudhuri and B. Mulder, Size and Shape of Excluded Volume Polymers Confined between Parallel Plates, *Phys. Rev. E: Stat., Nonlinear, Soft Matter Phys.*, 2011, **83**, 031803, DOI: **10.1103/PhysRevE.83.031803**.

54 D. Richter and M. Kruteva, Polymer Dynamics under Confinement, *Soft Matter*, 2019, **15**, 7316–7349, DOI: **10.1039/c9sm01141b**.

55 S. K. Dishari and M. A. Hickner, Antiplasticization and Water Uptake of Nafion® Thin Films, *ACS Macro Lett.*, 2012, **1**, 291–295, DOI: **10.1021/mz200169a**.

56 M. Tesfaye, A. N. MacDonald, P. J. Dudenas, A. Kusoglu and A. Z. Weber, Exploring Substrate/Ionomer Interaction under Oxidizing and Reducing Environments, *Electrochem. Commun.*, 2018, **87**, 86–90, DOI: **10.1016/j.elecom.2018.01.004**.

57 A. Ohira, S. Kuroda, H. F. M. Mohamed and B. Tavernier, Effect of Interface on Surface Morphology and Proton Conduction of Polymer Electrolyte Thin Films, *Phys. Chem. Chem. Phys.*, 2013, **15**, 11494–11500, DOI: **10.1039/c3cp51136g**.

58 T. Kawamoto, M. Aoki, T. Kimura, P. Chinapang, T. Mizusawa, N. L. Yamada, F. Nemoto, T. Watanabe, H. Tanida, M. Matsumoto, H. Imai, J. Miyake, K. Miyatake and J. Inukai, Sublayered Structures of Hydrated Nafion® Thin Film Formed by Casting on Pt Substrate Analyzed by X-Ray Absorption Spectroscopy under Ambient Conditions and Neutron Reflectometry at Temperature of 80 °C and Relative Humidity of 30-80%, *Electrochemistry*, 2019, **87**, 270–275, DOI: **10.5796/electrochemistry.19-00042**.

59 S. Poojary, M. N. Islam, U. N. Shrivastava, E. P. L. Roberts and K. Karan, Transport and Electrochemical Interface Properties of Ionomers in Low-Pt Loading Catalyst Layers: Effect of Ionomer Equivalent Weight and Relative Humidity, *Molecules*, 2020, **25**, 1–14, DOI: **10.3390/molecules25153387**.

60 A. Kusoglu, D. Kushner, D. K. Paul, K. Karan, M. A. Hickner and A. Z. Weber, Impact of Substrate and Processing on Confinement of Nafion Thin Films, *Adv. Funct. Mater.*, 2014, **24**, 4763–4774, DOI: **10.1002/adfm.201304311**.

61 D. I. Kushner, A. Kusoglu, N. J. Podraza and M. A. Hickner, Substrate-Dependent Molecular and Nanostructural Orientation of Nafion Thin Films, *Adv. Funct. Mater.*, 2019, **29**, 1–10, DOI: **10.1002/adfm.201902699**.

62 I. Yagi, K. Inokuma, K. Kimijima and H. Notsu, Molecular Structure of Buried Perfluorosulfonated Ionomer/Pt Interface Probed by Vibrational Sum Frequency Generation Spectroscopy, *J. Phys. Chem. C*, 2014, **118**, 26182–26190, DOI: **10.1021/jp5083592**.

63 D. L. W. Iii, J. Chlistunoff, J. Majewski and R. L. Borup, Nafion Structural Phenomena at Platinum and Carbon Interfaces, *J. Am. Chem. Soc.*, 2009, **131**, 18096–18104, DOI: **10.1021/ja9033928**.

64 J. L. Keddie, R. A. L. Jones and R. A. Cory, Interface and Surface Effects on the Glass-Transition Temperature in Thin Polymer Films, *Faraday Discuss.*, 1994, **98**, 219–230, DOI: **10.1039/fd9949800219**.

65 A. Kusoglu, T. J. Dursch and A. Z. Weber, Nanostructure/Swelling Relationships of Bulk and Thin-Film PFSA Ionomers, *Adv. Funct. Mater.*, 2016, **26**, 4961–4975, DOI: **10.1002/adfm.201600861**.

66 A. Kusoglu, in Ionomer Thin Films in PEM Fuel Cells, *Fuel Cells and Hydrogen Production*, ed. Lipman, T. E., Weber, A. Z., Springer, 2019, pp. 417–438, DOI: **10.1007/978-1-4939-7789-5_1021**.

67 C. Rotella, S. Naoplitano, L. D. Cremer, G. Koechelberghs and M. Wubbenhorst, Distribution of Segmental Mobility in Ultrathin Polymer Films, *Macromolecules*, 2010, **43**, 8686–8691, DOI: **10.1021/ma101695y**.

68 Y. Nie, Z. Zhou, T. Hao, X. Ye and W. Yang, The Distribution of Glass Transition Temperatures in Ultrathin Polymer Films Controlled by Segment Density or Interfacial Interaction, *Macromol. Theory Simul.*, 2016, **25**, 187–195, DOI: **10.1002/mats.201500062**.

69 E. C. Glor, G. V. Angrand and Z. Fakhraai, Exploring the Broadening and the Existence of Two Glass Transitions Due to Competing Interfacial Effects in Thin, Supported Polymer Films, *J. Chem. Phys.*, 2017, **146**, 1–11, DOI: **10.1063/1.4979944**.

70 S. Farzin, T. J. Johnson, S. Chatterjee, E. Zamani and S. K. Dishari, Ionomers From Kraft Lignin for Renewable Energy Applications, *Front. Chem.*, 2020, **8**, 1–17, DOI: **10.3389/fchem.2020.00690**.

71 Z. Su, S. Kole, L. C. Harden, V. M. Palakkal, C. Kim, G. Nair, C. G. Arges and J. N. Renner, Peptide-Modified Electrode Surfaces for Promoting Anion Exchange Ionomer Microphase Separation and Ionic Conductivity, *ACS Mater. Lett.*, 2019, **1**, 467–475, DOI: **10.1021/acsmaterialslett.9b00173**.

72 X. Gao, K. Yamamoto, T. Hirai, N. Ohta, T. Uchiyama, T. Watanabe, M. Takahashi, N. Takao, H. Imai, S. Sugawara, K. Shinohara and Y. Uchimoto, Substrate-Dependent Proton Transport and Nanostructural Orientation of Perfluorosulfonic Acid Polymer Thin Films on Pt and Carbon Substrate, *Solid State Ionics*, 2020, **357**, 1–7, DOI: **10.1016/j.ssi.2020.115456**.

73 J. A. Dura, V. S. Murthi, M. Hartman, S. K. Satija and C. F. Majkrzak, Multilamellar Interface Structures in Nafion, *Macromolecules*, 2009, **42**, 4769–4774, DOI: **10.1021/ma802823j**.

74 S. C. DeCaluwe, A. M. Baker, P. Bhargava, J. E. Fischer and J. A. Dura, Structure-Property Relationships at Nafion Thin-Film Interfaces: Thickness Effects on Hydration and Anisotropic Ion Transport, *Nano Energy*, 2018, **46**, 91–100, DOI: **10.1016/j.nanoen.2018.01.008**.

75 S. K. Dishari, C. A. Rumble, M. Maroncelli, J. A. Dura and M. A. Hickner, Unraveling the Complex Hydration Behavior of Ionomers under Thin Film Confinement, *J. Phys. Chem. C*, 2018, **122**, 3471–3481, DOI: **10.1021/acsmacrolett.1c00110**.

76 C. R. Randall, L. Zou, H. Wang, J. Hui, J. Rodríguez-López, M. Chen-Glasser, J. A. Dura and S. C. DeCaluwe, Morphology of Thin-Film Nafion on Carbon as an Analogue of Fuel Cell Catalyst Layers, *ACS Appl. Mater. Interfaces*, 2024, **16**, 3311–3324, DOI: **10.1021/acsami.3c14912**.

77 T. Kawamoto, T. Kimura, T. Mizusawa, N. L. Yamada, J. Miyake, K. Miyatake and J. Inukai, In-Plane Distribution of Water inside Nafion Thin Film Analyzed by Neutron Reflectivity at Temperature of 80 °C and Relative Humidity of 30%-80% Based on 4-Layered Structural Model, *Jpn. J. Appl. Phys.*, 2019, **58**, 1–5, DOI: **10.7567/1347-4065/ab0c7c**.

78 U. N. Shrivastava, K. Suetsugu, S. Nagano, H. Fritzsche, Y. Nagao and K. Karan, Cross-Correlated Humidity-Dependent Structural Evolution of Nafion Thin Films Confined on a Platinum Substrate, *Soft Matter*, 2020, **16**, 1190–1200, DOI: **10.1039/c9sm01731c**.

79 C. J. Ellison and J. M. Torkelson, The Distribution of Glass-Transition Temperatures in Nanoscopically Confined Glass Formers, *Nat. Mater.*, 2003, **2**, 695–700, DOI: **10.1038/nmat980**.

80 C. J. Ellison, S. D. Kim, D. B. Hall and J. M. Torkelson, Confinement and Processing Effects on Glass Transition Temperature and Physical Aging in Ultrathin Polymer Films: Novel Fluorescence Measurements, *Eur. Phys. J. E*, 2002, **8**, 155–166, DOI: **10.1140/epje/i2001-10057-y**.

81 M. K. Mundra, S. K. Donthu and V. P. Dravid, Effect of Spatial Confinement on the Glass-Transition Temperature of Patterned Polymer Nanostructures, *Nano Lett.*, 2007, **7**, 713–718, DOI: **10.1021/nl062894c**.

82 Y. Huang and D. R. Paul, Effect of Molecular Weight and Temperature on Physical Aging of Thin Glassy Poly(2,6-Dimethyl-1,4-Phenylene Oxide) Films, *J. Polym. Sci., Part B: Polym. Phys.*, 2007, **45**, 1390–1398, DOI: **10.1002/polb**.

83 G. B. Mckenna, in Dynamics of Materials at the Nanoscale: Small-Molecule Liquids and Polymer Films, *Polymer Physics:From Suspensions to Nanocomposites and Beyond*, ed. Utracki, L. A., Jamieson, A. M., John Wiley & Sons, Inc, 2010, pp. 191–223.

84 R. D. Priestley, L. J. Broadbelt and J. M. Torkelson, Physical Aging of Ultrathin Polymer Films above and below the Bulk Glass Transition Temperature: Effects of Attractive vs Neutral Polymer-Substrate Interactions Measured by Fluorescence, *Macromolecules*, 2005, **38**, 654–657, DOI: **10.1021/ma047994o**.

85 M. D. Fayer, Dynamics of Water Interacting with Interfaces, Molecules, and Ions, *Acc. Chem. Res.*, 2012, **45**, 3–14, DOI: **10.1021/ar2000088**.

86 M. D. Fayer and N. E. Levinger, Analysis of Water in Confined Geometries and at Interfaces, *Annu. Rev. Anal. Chem.*, 2010, **3**, 89–107, DOI: **10.1146/annurev-anchem-070109-103410**.

87 D. B. Spry, A. Goun, K. Glusac, D. E. Moilanen and M. D. Fayer, Proton Transport and the Water Environment in Nafion Fuel Cell Membranes and AOT Reverse Micelles, *J. Am. Chem. Soc.*, 2007, **129**, 8122–8130, DOI: **10.1021/ja071939o**.

88 J. M. Baker, J. C. Dore, J. M. Seddon and A. K. Soper, Structural Modification of Water in the Confined Layer of a Lamellar Lipid Crystal, *Chem. Phys. Lett.*, 1996, **256**, 649–652, DOI: **10.1016/0009-2614(96)00494-0**.

89 R. D. Priestley, Structural Relaxation of Polymer Glasses at Surfaces, Interfaces, and In Between, *Science*, 2005, **309**, 456–459, DOI: **10.1126/science.1112217**.

90 D. E. Moilanen, D. B. Spry and M. D. Fayer, Water Dynamics and Proton Transfer in Nafion Fuel Cell Membranes, *Langmuir*, 2008, **24**, 3690–3698, DOI: **10.1021/la703358a**.

91 J. Han and K. Burgess, Fluorescent Indicators for Intracellular PH, *Chem. Rev.*, 2010, **110**, 2709–2728, DOI: **10.1021/cr900249z**.

92 B. R. Frieberg, K. A. Page, J. R. Graybill, M. L. Walker, C. M. Stafford, G. R. Stafford and C. L. Soles, Mechanical Response of Thermally Annealed Nafion Thin Films, *ACS Appl. Mater. Interfaces*, 2016, **8**, 33240–33249, DOI: **10.1021/acsami.6b12423**.

93 N. J. Economou, A. M. Barnes, A. J. Wheat, M. S. Schaberg, S. J. Hamrock and S. K. Buratto, Investigation of Humidity Dependent Surface Morphology and Proton Conduction in Multi-Acid Side Chain Membranes by Conductive Probe Atomic Force Microscopy, *J. Phys. Chem. B*, 2015, **119**, 14280–14287, DOI: **10.1021/acs.jpcb.5b07255**.

94 J. J. Sumner, S. E. Creager, J. J. Ma and D. D. DesMarteau, Proton Conductivity in Nafion 117 and in a Novel Bis[(Perfluoroalkyl)Sulfonyl]Imide Ionomer Membrane, *J. Electrochem. Soc.*, 1998, **145**, 107–110, DOI: **10.1149/1.1838220**.

95 I. A. Koppel, R. W. Taft, F. Anvia, S. Z. Zhu, L. Q. Hu, K. S. Sung, D. D. DesMarteau, L. M. Yagupolskii, Y. L. Yagupolskii, N. V. Ignat'ev, N. V. Kondratenko, A. Y. Volkonskii, V. M. Vlasov, R. Notario and P. C. Maria, The Gas-Phase Acidities of Very Strong Neutral Brønsted Acids, *J. Am. Chem. Soc.*, 1994, **116**, 3047–3057, DOI: **10.1021/ja00086a038**.

96 S. K. Dishari, Current Understanding of Proton Conduction in Confined Ionomeric Systems, *J. Postdoc. Res.*, 2014, **2**, 30–39.

97 H. B. Park, H.-S. Shin, Y. M. Lee and J.-W. Rhim, Annealing Effect of Sulfonated Polysulfone Ionomer Membranes on Proton Conductivity and Methanol Transport, *J. Mem. Sci.*, 2005, **247**, 103–110, DOI: **10.1016/j.memsci.2004.09.023**.

98 K. A. Sung, W. Kim, K. Oh and J. Park, The Catalyst Layer Containing Sulfonated Poly (Ether Ether Ketone) as the Electrode Ionomer for Polymer Electrolyte Fuel Cells, *Electrochim. Acta*, 2009, **54**, 3446–3452, DOI: **10.1016/j.electacta.2009.01.024**.

99 J. S. Park, P. Krishnan, S. H. Park, G. G. Park, T. H. Yang, W. Y. Lee and C. S. Kim, A Study on Fabrication of Sulfonated Poly(Ether Ether Ketone)-Based Membrane-Electrode Assemblies for Polymer Electrolyte Membrane Fuel Cells, *J. Power Sources*, 2008, **178**, 642–650, DOI: **10.1016/j.jpowsour.2007.08.008**.

100 E. B. Easton, T. D. Astill and S. Holdcroft, Properties of Gas Diffusion Electrodes Containing Sulfonated Poly (Ether Ether Ketone), *J. Electrochem. Soc.*, 2005, **152**, A752–A758, DOI: **10.1149/1.1864412**.

101 W. K. Kim, K. A. Sung, K. H. Oh, M. J. Choo, K. Y. Cho, K. Y. Cho and J. K. Park, A New Catalyst Layer Based on in Situ Pore Generation of Sulfonated Poly(Ether Ether Ketone) for PEMFC, *Electrochem. Commun.*, 2009, **11**, 1714–1716, DOI: **10.1016/j.elecom.2009.07.003**.

102 J. Peron, D. Edwards, A. Besson, Z. Shi and S. Holdcroft, Microstructure-Performance Relationships of SPEEK-Based Catalyst Layers, *J. Electrochem. Soc.*, 2010, **157**, B1230–B1236, DOI: **10.1149/1.3454735**.

103 T. Astill, Z. Xie, Z. Shi, T. Navessin and S. Holdcroft, Factors Influencing Electrochemical Properties and Performance of Hydrocarbon-Based Electrolyte PEMFC Catalyst Layers, *J. Electrochem. Soc.*, 2009, **156**, B499–B508, DOI: **10.1149/1.3082119**.

104 C. Ma, L. Zhang, S. Mukerjee, D. Ofer and B. Nair, An Investigation of Proton Conduction in Select PEM's and Reaction Layer Interfaces-Designed for Elevated Temperature Operation, *J. Mem. Sci.*, 2003, **219**, 123–136, DOI: **10.1016/S0376-7388(03)00194-7**.

105 K. H. Lim, A. S. Lee, V. Atanasov, J. Kerres, E. J. Park, S. Adhikari, S. Maurya, L. D. Manriquez, J. Jung, C. Fujimoto, I. Matanovic, J. Jankovic, Z. Hu, H. Jia and Y. S. Kim, Protonated Phosphonic Acid Electrodes for High Power Heavy-Duty Vehicle Fuel Cells, *Nat. Energy*, 2022, **7**, 248–259, DOI: **10.1038/s41560-021-00971-x**.

106 E. O. Balogun, N. Hussain, J. Chamier and P. Barendse, Performance and Durability Studies of Perfluorosulfonic Acid Ionomers as Binders in PEMFC Catalyst Layers Using Electrochemical Impedance Spectroscopy, *Int. J. Hydrogen Energy*, 2019, **44**, 32219–32230, DOI: **10.1016/j.ijhydene.2019.10.079**.

107 S. V. Kraemer, G. Lindbergh, B. Lafitte, M. Puchner and P. Jannasch, Substitution of Nafion with Sulfonated Polysulfone in Membrane–Electrode Assembly Components for 60–120 °C PEMFC Operation, *J. Electrochem. Soc.*, 2008, **155**, 1–8, DOI: **10.1149/1.2959113**.

108 V. Ramani, S. Swier, M. T. Shaw, R. A. Weiss, H. R. Kunz and J. M. Fenton, Membranes and MEAs Based on Sulfonated Poly(Ether Ketone Ketone) and Heteropolyacids for Polymer Electrolyte Fuel Cells, *J. Electrochem. Soc.*, 2008, **155**, 1–7, DOI: **10.1149/1.2898171**.

109 K. Miyatake, H. Uchida and M. Watanabe, Gas Diffusion Electrodes Containing Sulfonated Polyether Ionomers for PEFCs, *Electrochim. Acta*, 2007, **53**, 1972–1978, DOI: **10.1016/j.electacta.2007.08.054**.

110 T. Yoda, T. Shimura, B. Bae, K. Miyatake, H. Uchida and M. Watanabe, Gas Diffusion Electrodes Containing Sulfonated Poly (Arylene Ether) Ionomer for Polymer Electrolyte Fuel Cells Part 2. Improvement of the Cathode Performance, *Electrochim. Acta*, 2010, **55**, 3464–3470, DOI: **10.1016/j.electacta.2009.12.046**.

111 F. Wang, M. Hickner, Q. Ji, W. Harrison, J. Mecham, T. A. Zawodzinski and J. E. McGrath, Synthesis of Highly Sulfonated Poly(Arylene Ether Sulfone) Random (Statisical) Copolymers via Direct Polymerization, *Macromol. Symp.*, 2001, **175**, 387–395.

112 J. E. Chae, S. J. Yoo, J. Y. Kim, J. H. Jang, S. Y. Lee, K. H. Song and H. J. Kim, Hydrocarbon-Based Electrode Ionomer for Proton Exchange Membrane Fuel Cells, *Int. J. Hydrogen Energy*, 2020, **45**, 32856–32864, DOI: **10.1016/j.ijhydene.2020.03.003**.

113 N. N. Krishnan, H. Kim, J. H. Jang, S. Lee and E. Cho, Sulfonated Poly (Ether Sulfone)-Based Catalyst Binder for a Proton-Exchange Membrane Fuel Cell, *J. Appl. Polym. Sci.*, 2009, **113**, 2499–2506, DOI: **10.1002/app.30296**.

114 T. J. G. Skalski, M. Adamski, B. Britton, E. M. Schibli, T. J. Peckham, T. Weissbach, T. Moshisuki, S. Lyonnard, B. J. Frisken and S. Holdcroft, Sulfophenylated Terphenylene Copolymer Membranes and Ionomers, *ChemSusChem*, 2018, **11**, 4033–4043, DOI: **10.1002/cssc.201801965**.

115 E. Balogun, P. Mardle, H. Nguyen, M. Breitwieser and S. Holdcroft, Catalyst Layers for Fluorine-Free Hydrocarbon PEMFCs, *Electrochim. Acta*, 2022, **401**, 1–13, DOI: **10.1016/j.electacta.2021.139479**.

116 E. Higuchi, K. Okamoto, K. Miyatake, H. Uchida and M. Watanabe, Gas Diffusion Electrodes for Polymer Electrolyte Fuel Cell Using Sulfonated Polyimide, *Res. Chem. Intermed.*, 2006, **32**, 533–542, DOI: **10.1163/156856706777973781**.

117 M. Hwang, K. Nixon, R. Sun, C. Willis and Y. A. Elabd, Sulfonated Pentablock Terpolymers as Membranes and Ionomers in Hydrogen Fuel Cells, *J. Mem. Sci.*, 2021, **633**, 1–11, DOI: **10.1016/j.memsci.2021.119330**.

118 H. Nguyen, F. Lombeck, C. Schwarz, P. A. Heizmann, M. Adamski, H. Lee, B. Britton, S. Holdcroft, S. Vierrath and M. Breitwieser, Hydrocarbon-Based Pemion™ Proton Exchange Membrane Fuel Cells with State-of-the-Art Performance, *Sustain. Energy Fuels*, 2021, **5**, 3687–3699, DOI: **10.1039/d1se00556a**.

119 J. Eon, B. Hyun, J. Hyun, J. Jung, J. Kim, J. Hyun, S. Jong, H. Kim and S. Young, Effect of the Spirobiindane Group in Sulfonated Poly (Arylene Ether Sulfone) Copolymer as Electrode Binder for Polymer Electrolyte Membrane Fuel Cells, *J. Ind. Eng. Chem.*, 2017, **47**, 315–322, DOI: **10.1016/j.jiec.2016.11.047**.

120 Q. Zhang, S. Dong, P. Shao, Y. Zhu, Z. Mu, D. Sheng, T. Zhang, X. Jiang, R. Shao, Z. Ren, J. Xie, X. Feng and B. Wang, Covalent Organic Framework-Based Porous Ionomers for High-Performance Fuel Cells, *Science*, 2022, **378**, 181–186, DOI: **10.1126/science.abm6304**.

121 D. B. Spry and M. D. Fayer, Proton Transfer and Proton Concentrations in Protonated Nafion Fuel Cell Membranes, *J. Phys. Chem. B*, 2009, **113**, 10210–10221, DOI: **10.1021/jp9036777**.

122 K. D. Kreuer, On the Development of Proton Conducting Polymer Membranes for Hydrogen and Methanol Fuel Cells, *J. Mem. Sci.*, 2001, **185**, 29–39, DOI: **10.1016/S0376-7388(00)00632-3**.

123 K. Kreuer, S. J. Paddison, E. Spohr and M. Schuster, Transport in Proton Conductors for Fuel-Cell Applications: Simulations, Elementary Reactions, and Phenomenology, *Chem. Rev.*, 2004, **104**, 4637–4678, DOI: **10.1021/cr020715f**.

124 K. A. Page, A. Kusoglu, C. M. Sta, S. Kim, R. J. Kline and A. Z. Weber, Confinement-Driven Increase in Ionomer Thin-Film Modulus, *Nano Lett.*, 2014, **14**, 2299–2304, DOI: **10.1021/nl501233g**.

125 T. J. Zimudzi and M. A. Hickner, Signal Enhanced FTIR Analysis of Alignment in NAFION Thin Films at SiO2 and Au Interfaces, *ACS Macro Lett.*, 2016, **5**, 83–87, DOI: **10.1021/acsmacrolett.5b00800**.

126 J. H. Lee, H. Kang, S. D. Yim, Y. J. Sohn and S. G. Lee, Revelation of Transport Properties of Ultra-Thin Ionomer Films in Catalyst Layer of Polymer Electrolyte Membrane Fuel Cells Using Molecular Dynamics, *Appl. Surf. Sci.*, 2022, **598**, 1–10, DOI: **10.1016/j.apsusc.2022.153815**.

127 S. Takahashi, J. Shimanuki, T. Mashio, A. Ohma, H. Tohma, A. Ishihara, Y. Ito, Y. Nishino and A. Miyazawa, Observation of Ionomer in Catalyst Ink of Polymer Electrolyte Fuel Cell Using Cryogenic Transmission Electron Microscopy, *Electrochim. Acta*, 2017, **224**, 178–185, DOI: **10.1016/j.electacta.2016.12.068**.

128 S. A. Eastman, S. Kim, K. A. Page, B. W. Rowe, S. Kang, C. L. Soles and K. G. Yager, Effect of Confinement on Structure, Water Solubility, and Water Transport in Nafion Thin Films, *Macromolecules*, 2012, **45**, 7920–7930, DOI: **10.1021/ma301289v**.

129 V. S. Murthi, J. A. Dura, S. Satija and C. F. Majkrzak, Water Uptake and Interfacial Structural Changes of Thin Film Nafion Membranes Measured by Neutron Reflectivity for PEM Fuel Cells, *ECS Trans.*, 2008, **16**, 1471–1485, DOI: **10.1149/1.2981988**.

130 D. Mckechnie, J. Cree, D. Wadkin-snaith and K. Johnston, Glass Transition Temperature of a Polymer Thin Film: Statistical and Fitting Uncertainties, *Polymer*, 2020, **195**(1–7), 122433, DOI: **10.1016/j.polymer.2020.122433**.

131 S. C. DeCaluwe, P. A. Kienzle, P. Bhargava, A. M. Baker and J. A. Dura, Phase Segregation of Sulfonate Groups in Nafion Interface Lamellae, Quantified via Neutron Reflectometry Fitting Techniques for Multi-Layered Structures, *Soft Matter*, 2014, **10**, 5763–5776, DOI: **10.1039/c4sm00850b**.

132 K. Kodama, K. Motobayashi, A. Shinohara, N. Hasegawa, K. Kudo, R. Jinnouchi, M. Osawa and Y. Morimoto, Effect of the Side-Chain Structure of Perfluoro-Sulfonic Acid Ionomers on the Oxygen Reduction Reaction on the Surface of Pt, *ACS Catal.*, 2018, **8**, 694–700, DOI: **10.1021/acscatal.7b03571**.

133 G. S. Hwang, D. Y. Parkinson, A. Kusoglu, A. A. MacDowell and A. Z. Weber, Understanding Water Uptake and Transport in Nafion Using X-Ray Microtomography, *ACS Macro Lett.*, 2013, **2**, 288–291, DOI: **10.1021/mz300651a**.

134 S. K. Babu, H. T. Chung, P. Zelenay and S. Litster, Resolving Electrode Morphology's Impact on Platinum Group Metal-Free Cathode Performance Using Nano-CT of 3D Hierarchical Pore and Ionomer Distribution, *ACS Appl. Mater. Interfaces*, 2016, **8**, 32764–32777, DOI: **10.1021/acsami.6b08844**.

135 F. I. Allen, L. R. Comolli, A. Kusoglu, M. A. Modestino, A. M. Minor and A. Z. Weber, Morphology of Hydrated As-Cast Nafion Revealed through Cryo Electron Tomography, *ACS Macro Lett.*, 2015, **4**, 1–5, DOI: **10.1021/mz500606h**.

136 C. Wang, D. H. Lee, A. Hexemer, M. I. Kim, W. Zhao, H. Hasegawa, H. Ade and T. P. Russell, Defining the Nanostructured Morphology of Triblock Copolymers Using Resonant Soft X-Ray Scattering, *Nano Lett.*, 2011, **11**, 3906–3911, DOI: **10.1021/nl2020526**.

137 T. E. Culp, D. Ye, M. Paul, A. Roy, M. J. Behr, S. Jons, S. Rosenberg, C. Wang, E. W. Gomez, M. Kumar and E. D. Gomez, Probing the Internal Microstructure of Polyamide Thin-Film Composite Membranes Using Resonant Soft X-Ray Scattering, *ACS Macro Lett.*, 2018, **7**, 927–932, DOI: **10.1021/acsmacrolett.8b00301**.

138 F. Liu, M. A. Brady and C. Wang, Resonant Soft X-Ray Scattering for Polymer Materials, *Eur. Polym. J.*, 2016, **81**, 555–568, DOI: **10.1016/j.eurpolymj.2016.04.014**.

139 C. B. Roth, K. L. Mcnerny, W. F. Jager and J. M. Torkelson, Eliminating the Enhanced Mobility at the Free Surface of Polystyrene: Fluorescence Studies of the Glass Transition Temperature in Thin Bilayer Films of Immiscible Polymers, *Macromolecules*, 2007, **40**, 2568–2574, DOI: **10.1021/ma062864w**.

140 R. R. Baglay and C. B. Roth, Local Glass Transition Temperature Tg (z) of Polystyrene next to Different Polymers: Hard vs. Soft Confinement, *J. Chem. Phys.*, 2017, **146**(1–13), 203307, DOI: **10.1063/1.4975168**.

141 N. A. García and J. L. Barrat, Entanglement Reduction Induced by Geometrical Confinement in Polymer Thin Films, *Macromolecules*, 2018, **51**, 9850–9860, DOI: **10.1021/acs.macromol.8b01884**.

142 I. Siretanu, J. P. Chapel and C. Drummond, Substrate Remote Control of Polymer Film Surface Mobility, *Macromolecules*, 2012, **45**, 1001–1005, DOI: **10.1021/ma202187s**.

143 N. E. D. Almeida, D. K. Paul, K. Karan and G. R. Goward, 1H Solid-State NMR Study of Nanothin Nafion Films, *J. Phys. Chem. C*, 2015, **119**, 1280–1285, DOI: **10.1021/jp5086747**.

144 T. A. M. Suter, K. Smith, J. Hack, L. Rasha, Z. Rana, G. M. A. Angel, P. R. Shearing, T. S. Miller and D. J. L. Brett, Engineering Catalyst Layers for Next-Generation Polymer Electrolyte Fuel Cells: A Review of Design, Materials, and Methods, *Adv. Energy Mater.*, 2021, **11**, 1–82, DOI: **10.1002/aenm.202101025**.

145 A. Ohma, K. Fushinobu and K. Okazaki, Influence of Nafion® Film on Oxygen Reduction Reaction and Hydrogen Peroxide Formation on Pt Electrode for Proton Exchange Membrane Fuel Cell, *Electrochim. Act.*, 2010, **55**, 8829–8838, DOI: **10.1016/j.electacta.2010.08.005**.

146 J. Tymoczko, F. Calle-Vallejo, V. Colic, M. T. M. Koper, W. Schuhmann and A. S. Bandarenka, Oxygen Reduction at a Cu-Modified Pt(111) Model Electrocatalyst in Contact with Nafion Polymer, *ACS Catal.*, 2014, **4**, 3772–3778, DOI: **10.1021/cs501037y**.

147 Z. Xu, S. Yuan, L. An, S. Shen, Q. Xu, X. Yan and J. Zhang, Effect of Substrate Surface Charges on Proton Conduction of Ultrathin Nafion Films, *ACS Appl. Mater. Interfaces*, 2023, **15**, 10735–10743, DOI: **10.1021/acsami.2c21977**.

148 S. Ott, F. Du, M. L. Luna, T. A. Dao, B. R. Cuenya, A. Orfanidi and P. Strasser, Understanding the Performance Increase of Catalysts Supported on N-Functionalized Carbon in PEMFC Catalyst Layers, *J. Electrochem. Soc.*, 2022, **169**, 1–14, DOI: **10.1149/1945-7111/ac6e4d**.

149 M. A. Modestino, A. Kusoglu, A. Hexemer, A. Z. Weber and R. A. Segalman, Controlling Nafion Structure and Properties via Wetting Interactions, *Macromolecules*, 2012, **45**, 4681–4688, DOI: **10.1021/ma300212f**.

150 G. Doo, S. Yuk, J. H. Lee, S. Choi, D. H. Lee, D. W. Lee, J. Hyun, S. H. Kwon, S. G. Lee and H. T. Kim, Nano-Scale Control of the Ionomer Distribution by Molecular Masking of the Pt Surface in PEMFCs, *J. Mater. Chem. A*, 2020, **8**, 13004–13013, DOI: **10.1039/c9ta14002f**.

151 Y. Li, J. Hart, L. Profitt, S. Intikhab, S. Chatterjee, M. Taheri and J. Snyder, Sequential Capacitive Deposition of Ionic Liquids for Conformal Thin Film Coatings on Oxygen Reduction Reaction Electrocatalysts, *ACS Catal.*, 2019, **9**, 9311–9316, DOI: **10.1021/acscatal.9b03157**.

152 R. Friedmann and T. Van Nguyen, Optimization of the Microstructure of the Cathode Catalyst Layer of a PEMFC for Two-Phase Flow, *J. Electrochem. Soc.*, 2010, **157**, 1–7, DOI: **10.1149/1.3264628**.

153 R. P. Dowd, C. S. Day and T. Van Nguyen, Engineering the Ionic Polymer Phase Surface Properties of a PEM Fuel Cell Catalyst Layer, *J. Electrochem. Soc.*, 2017, **164**, F138–F146, DOI: **10.1149/2.1081702jes**.

154 Y. Yang, C. Zhao, Z. Wang, X. Fan and C. Yan, Synergistic Effects of N-Doping and Mesoporous Structures in Block Copolymer-Derived Three-Dimensionally Ordered Mesoporous Carbon for PEMFC, *Int. J. Hydrogen Energy*, 2024, **51**, 747–757, DOI: **10.1016/j.ijhydene.2023.10.197**.

155 Y. Li, S. Intikhab, A. Malkani, B. Xu and J. Snyder, Ionic Liquid Additives for the Mitigation of Nafion Specific Adsorption on Platinum, *ACS Catal.*, 2020, **10**, 7691–7698, DOI: **10.1021/acscatal.0c01243**.

156 G. R. Zhang, T. Wolker, D. J. S. Sandbeck, M. Munoz, K. J. J. Mayrhofer, S. Cherevko and B. J. M. Etzold, Tuning the Electrocatalytic Performance of Ionic Liquid Modified Pt Catalysts for the Oxygen Reduction Reaction via Cationic Chain Engineering, *ACS Catal.*, 2018, **8**, 8244–8254, DOI: **10.1021/acscatal.8b02018**.

157 A. Avid, J. L. Ochoa, Y. Huang, Y. Liu, P. Atanassov and I. V. Zenyuk, Revealing the Role of Ionic Liquids in Promoting Fuel Cell Catalysts Reactivity and Durability, *Nat. Commun.*, 2022, **13**, 1–13, DOI: **10.1038/s41467-022-33895-5**.

158 K. Brunnengräber, K. Jeschonek, M. George, G. Zhang and B. J. M. Etzold, Ionic Liquid Modified Electrocatalysts: A STEM-EDX Approach for Identification of Local Distributions within Ionomer Containing Catalysts Layers, *Chem. Methods*, 2023, 1–9, DOI: **10.1002/cmtd.202200084**.

159 R. Sun, M. Agrawal, K. C. Neyerlin, J. D. Snyder and Y. A. Elabd, Proton Conducting Sulfonated Poly(Ionic Liquid) Block Copolymers, *Macromolecules*, 2022, **55**, 6716–6729, DOI: **10.1021/acs.macromol.2c00468**.

160 R. Gawas, R. Sun, Y. Li, K. C. Neyerlin, Y. A. Elabd, M. Tang and J. Snyder, Characterization of a Sulfonated Poly(Ionic Liquid) Block Copolymer as an Ionomer for Proton Exchange Membrane Fuel Cells Using Rotating Disk Electrode, *J. Electrochem. Soc.*, 2021, **168**, DOI: **10.1149/1945-7111/ac4375**.

161 Z. Su, N. Pramounmat, S. T. Watson and J. N. Renner, Engineered Interaction between Short Elastin-like Peptides and Perfluorinated Sulfonic-Acid Ionomer, *Soft Matter*, 2018, **14**, 3528–3535, DOI: **10.1039/c8sm00351c**.

162 J. P. Coote, T. Kinsey, D. P. Street, S. M. Kilbey, J. R. Sangoro and G. E. Stein, Surface-Induced Ordering Depresses Through-Film Ionic Conductivity in Lamellar Block Copolymer Electrolytes, *ACS Macro Lett.*, 2020, **9**, 565–570, DOI: **10.1021/acsmacrolett.0c00039**.

163 Y. Ogata, T. Abe, S. Yonemori, N. L. Yamada, D. Kawaguchi and K. Tanaka, Impact of the Solid Interface on Proton Conductivity in Nafion Thin Films, *Langmuir*, 2018, **34**, 15483–15489, DOI: **10.1021/acs.langmuir.8b03396**.

164 C. H. Lee, W. J. M. Kort-Kamp, H. Yu, D. A. Cullen, B. M. Patterson, T. A. Arman, S. Komini Babu, R. Mukundan, R. L. Borup and J. S. Spendelow, Grooved Electrodes for High-Power-Density Fuel Cells, *Nat. Energy*, 2023, **8**, 685–694, DOI: **10.1038/s41560-023-01263-2**.

165 B. James, Cost Projections of PEM Fuel Cell Systems for Automobiles and Medium-Duty Vehicles (DOE-Fuel Cell Technologies Office), 2018, **https://www.energy.gov/eere/fuelcells/downloads/2018-cost-projections-pem-fuel-cell-systems-automobiles-and-medium-duty**.

166 S. U. Kim, D. M. Yu, T. H. Kim, Y. T. Hong, S. Y. Nam and J. H. Choi, Effect of Sulfonated Poly(Arylene Ether Sulfone) Binder on the Performance of Polymer Electrolyte Membrane Fuel Cells, *J. Ind. Eng. Chem.*, 2015, **23**, 316–320, DOI: **10.1016/j.jiec.2014.08.035**.

167 K. Ebata, T. Togashi, S. Yamamoto, M. Mitsuishi and J. Matsui, Self Formed Anisotropic Proton Conductive Polymer Film by Nano-phase Separation, *J. Electrochem. Soc.*, 2019, **166**, B3218–B3222, DOI: **10.1149/2.0331909jes**.

168 T. Sato, Y. Hayasaka, M. Mitsuishi, T. Miyashita, S. Nagano and J. Matsui, High Proton Conductivity in the Molecular Interlayer of a Polymer Nanosheet Multilayer Film, *Langmuir*, 2015, **31**, 5174–5180, DOI: **10.1021/acs.langmuir.5b00036**.

169 Y. Ono, R. Goto, M. Hara, S. Nagano, T. Abe and Y. Nagao, High Proton Conduction of Organized Sulfonated Polyimide Thin Films with Planar and Bent Backbones, *Macromolecules*, 2018, **51**, 3351–3359, DOI: **10.1021/acs.macromol.8b00301**.

170 Y. Nagao, J. Matsui, T. Abe, H. Hiramatsu, H. Yamamoto, T. Miyashita, N. Sata and H. Yugami, Enhancement of Proton Transport in an Oriented Polypeptide Thin Film, *Langmuir*, 2013, **29**, 6798–6804, DOI: **10.1021/la400412f**.

171 H. Yabu, J. Matsui, M. Hara, S. Nagano, Y. Matsuo and Y. Nagao, Proton Conductivities of Lamellae-Forming Bioinspired Block Copolymer Thin Films Containing Silver Nanoparticles, *Langmuir*, 2016, **32**, 9484–9491, DOI: **10.1021/acs.langmuir.6b02521**.

172 K. Takakura, Y. Ono, K. Suetsugu, M. Hara, S. Nagano, T. Abe and Y. Nagao, Lyotropic Ordering for High Proton Conductivity in Sulfonated Semialiphatic Polyimide Thin Films, *Polym. J.*, 2019, **51**, 31–39, DOI: **10.1038/s41428-018-0111-1**.

173 Y. Nagao, T. Tanaka, Y. Ono, K. Suetsugu, M. Hara, G. Wang, S. Nagano and T. Abe, Introducing Planar Hydrophobic Groups into an Alkyl-Sulfonated Rigid Polyimide and How This Affects Morphology and Proton Conductivity, *Electrochim. Acta*, 2019, **300**, 333–340, DOI: **10.1016/j.electacta.2019.01.118**.

174 K. Krishnan, H. Iwatsuki, M. Hara, S. Nagano and Y. Nagao, Proton Conductivity Enhancement in Oriented, Sulfonated Polyimide Thin Films, *J. Mater. Chem. A*, 2014, **2**, 6895–6903, DOI: **10.1039/c4ta00579a**.

175 Y. Nagao and J. Matsui, Anisotropic Proton Conductivity of Poly(Aspartic Acid) Thin Films, *Mater. Today Proc.*, 2019, **17**, 953–958, DOI: **10.1016/j.matpr.2019.06.448**.

176 E. B. Trigg, T. W. Gaines, M. Maréchal, D. E. Moed, P. Rannou, K. B. Wagener, M. J. Stevens and K. I. Winey, Self-Assembled Highly Ordered Acid Layers in Precisely Sulfonated Polyethylene Produce Efficient Proton Transport, *Nat. Mater.*, 2018, **17**, 725–731, DOI: **10.1038/s41563-018-0097-2**.

177 M. Tsuksamoto, K. Ebata, H. Sakiyama, S. Yamamoto, M. Mitsuishi, T. Miyashita and J. Matsui, Biomimetic Polyelectrolytes Based on Polymer Nanosheet Films and Their Proton Conduction Mechanism, *Langmuir*, 2019, **35**, 3302–3307, DOI: **10.1021/acs.langmuir.8b04079**.

178 G. Xu, K. Otsubo, T. Yamada, S. Sakaida and H. Kitagawa, Super-protonic Conductivity in a Highly Oriented Crystalline Metal-Organic Framework Nanofilm, *JACS*, 2013, **135**, 7438–7441, DOI: **10.1021/ja402727d**.

179 Y. S. Kim, M. A. Hickner, L. Dong, B. S. Pivovar and J. E. McGrath, Sulfonated Poly(Arylene Ether Sulfone) Copolymer Proton Exchange Membranes: Composition and Morphology Effects on the Methanol Permeability, *J. Mem. Sci.*, 2004, **243**, 317–326, DOI: **10.1016/j.memsci.2004.06.035**.

180 J. E. Cha, W. J. Cho, J. Hwang, D. J. Seo, Y. W. Choi and W. B. Kim, Fuel Cell Performance Improvement via the Steric Effect of a Hydrocarbon-Based Binder for Cathode in Proton Exchange Membrane Fuel Cells, *Sci. Rep.*, 2022, **12**, 1–8, DOI: **10.1038/s41598-022-18464-6**.

181 S. Farzin; K. A. Cerda; O. A. Obewhere and S. K. Dishari, in Lignin-Based Materials for Energy Conversion and Storage Devices, *Sustainability Engineering: Challenges, Technologies, and Applications*, ed. Tan, E. C., 2023, pp. 1–60, DOI: **10.1201/9781003167693-1**.

182 K. Acurio Cerda, M. Kathol, G. Purohit, E. Zamani, M. D. Morton, O. Khalimonchuk, R. Saha and S. K. Dishari, Cationic Lignin as an Efficient and Biorenewable Antimicrobial Material, *ACS Sustainable Chem. Eng.*, 2023, **11**, 10364–10379, DOI: **10.1021/acssuschemeng.3c01414**.

183 M. A. Abu-dalo, N. A. F. Al-rawashdeh and A. Ababneh, Evaluating the Performance of Sulfonated Kraft Lignin Agent as Corrosion Inhibitor for Iron-Based Materials in Water Distribution Systems, *Desalination*, 2013, **313**, 105–114, DOI: **10.1016/j.desal.2012.12.007**.

184 D. S. Bajwa, G. Pourhashem, A. H. Ullah and S. G. Bajwa, A Concise Review of Current Lignin Production, Applications, Products and Their Environment Impact, *Ind. Crop. Prod.*, 2019, **139**, 1–11, DOI: **10.1016/j.indcrop.2019.111526**.

185 C. Che, M. Vagin, K. Wijeratne, D. Zhao, M. Warczak, M. P. Jonsson and X. Crispin, Conducting Polymer Electrocatalysts for Proton-Coupled Electron Transfer Reactions: Toward Organic Fuel Cells with Forest Fuels, *Adv. Sustain. Syst.*, 2018, **2**, 1–7, DOI: **10.1002/adsu.201800021**.

186 A. L. Holmberg, J. F. Stanzione, R. P. Wool and T. H. Epps, A Facile Method for Generating Designer Block Copolymers from Functionalized Lignin Model Compounds, *ACS Sustain. Chem. Eng.*, 2014, **2**, 569–573, DOI: **10.1021/sc400497a**.

187 A. L. Holmberg, K. H. Reno, R. P. Wool and T. H. Epps, Biobased Building Blocks for the Rational Design of Renewable Block Polymers, *Soft Matter*, 2014, **10**, 7405–7424, DOI: **10.1039/c4sm01220h**.

188 W. Zhang, J. Yin, Z. Lin, H. Lin, H. Lu, Y. Wang and W. Huang, Facile Preparation of 3D Hierarchical Porous Carbon from Lignin for the Anode Material in Lithium Ion Battery with High Rate Performance, *Electrochim. Acta*, 2015, **176**, 1136–1142, DOI: **10.1016/j.electacta.2015.08.001**.

189 Y. Xi, Y. Wang, D. Yang, Z. Zhang, W. Liu, Q. Li and X. Qiu, K2CO3 Activation Enhancing the Graphitization of Porous Lignin Carbon Derived from Enzymatic Hydrolysis Lignin for High Performance Lithium-Ion Storage, *J. Alloys Compd.*, 2019, **785**, 706–714, DOI: **10.1016/j.jallcom.2019.01.039**.

190 Y. F. Du, G. H. Sun, Y. Li, J. Y. Cheng, J. P. Chen, G. Song, Q. Q. Kong, L. J. Xie and C. M. Chen, Pre-Oxidation of Lignin Precursors for Hard Carbon Anode with Boosted Lithium-Ion Storage Capacity, *Carbon*, 2021, **178**, 243–255, DOI: **10.1016/j.carbon.2021.03.016**.

191 Z. Yang, H. Guo, F. Li, X. Li, Z. Wang, L. Cui and J. Wang, Cooperation of Nitrogen-Doping and Catalysis to Improve the Li-Ion Storage Performance of Lignin-Based Hard Carbon, *J. Energy Chem.*, 2018, **27**, 1390–1396, DOI: **10.1016/j.jechem.2018.01.013**.

192 Z. Z. Chang, B. J. Yu and C. Y. Wang, Influence of H2 Reduction on Lignin-Based Hard Carbon Performance in Lithium Ion Batteries, *Electrochim. Acta*, 2015, **176**, 1352–1357, DOI: **10.1016/j.electacta.2015.07.076**.

193 L. Du, W. Wu, C. Luo, H. Zhao, D. Xu, R. Wang and Y. Deng, Lignin Derived Si@C Composite as a High Performance Anode Material for Lithium Ion Batteries, *Solid State Ionics*, 2018, **319**, 77–82, DOI: **10.1016/j.ssi.2018.01.039**.

194 J. Hayashi, A. Kazehaya, K. Muroyama and A. P. Watkinson, Preparation of Activated Carbon from Lignin by Chemical Activation, *Carbon*, 2000, **38**, 1873–1878, DOI: **10.1016/S0008-6223(00)00027-0**.

195 *2023 Billion-Ton Report: An Assessment of U.S. Renewable Carbon Resources by U.S. Department of Energy*. **https://www.energy.gov/sites/default/files/2024-03/beto-2023-billion-ton-report_1.pdf**.

196 K. Jie, Y. Zhou, Y. Yao and F. Huang, Macrocyclic Amphiphiles, *Chem. Soc. Rev.*, 2015, **44**, 3568–3587, DOI: **10.1039/C4CS00390J**.

197 K. Helttunen and P. Shahgaldian, Self-Assembly of Amphiphilic Calixarenes and Resorcinarenes in Water, *New J. Chem.*, 2010, **34**, 2704–2714, DOI: **10.1039/C0NJ00123F**.

198 S. Fujii, J. H. Lee, R. Takahashi and K. Sakurai, Rediscovering the Monodispersity of Sulfonatocalix[4]Arene-Based Micelles, *Langmuir*, 2018, **34**, 5072–5078, DOI: **10.1021/acs.langmuir.8b00802**.

199 G. M. L. Consoli; G. Granata and C. Geraci, *Calixarene-Based Micelles*, Elsevier Inc, 2018, , DOI: **10.1016/b978-0-12-813627-0.00003-x**.

200 R. H. Tunuguntla, F. I. Allen, K. Kim, A. Belliveau and A. Noy, Ultrafast Proton Transport in Sub-1-Nm Diameter Carbon Nanotube Porins, *Nat. Nanotechnol.*, 2016, **11**, 639–644, DOI: **10.1038/nnano.2016.43**.

201 Y. Li, Z. Li, F. Aydin, J. Quan, X. Chen, Y. C. Yao, C. Zhan, Y. Chen, T. A. Pham and A. Noy, Water-Ion Permselectivity of Narrow-Diameter Carbon Nanotubes, *Sci. Adv.*, 2020, **6**, 1–9, DOI: **10.1126/sciadv.aba9966**.

202 M. Akeson and D. W. Deamer, Proton Conductance by the Gramicidin Water Wire. Model for Proton Conductance in the F1F0 ATPases?, *Biophys. J.*, 1991, **60**, 101–109, DOI: **10.1016/S0006-3495(91)82034-3**.

203 M. Baaden, M. Barboiu, R. M. Bill, S. Casanova, C. L. Chen, M. Conner, V. Freger, B. Gong, A. Góra, B. Hinds, A. Horner, G. Hummer, M. Kumar, M. Lokesh, S. Mitra, A. Noy, P. Pohl, A. Sadet, M. Sansom, S. Törnroth-Horsefield and H. Vashisth, Structure and Function of Natural Proteins for Water Transport: General Discussion, *Faraday Discuss.*, 2018, **209**, 83–95, DOI: **10.1039/C8FD90019A**.

204 J. Pfeffermann, N. Goessweiner-Mohr and P. Pohl, The Energetic Barrier to Single-File Water Flow through Narrow Channels, *Biophys. Rev.*, 2021, **13**, 913–923, DOI: **10.1007/s12551-021-00875-w**.

205 R. Epsztein, R. M. DuChanois, C. L. Ritt, A. Noy and M. Elimelech, Towards Single-Species Selectivity of Membranes with Subnanometre Pores, *Nat. Nanotechnol.*, 2020, **15**, 426–436, DOI: **10.1038/s41565-020-0713-6**.

206 H. Wang, C. Yang, S. Wang and S. Hu, Tunable Ion Transport through Ultimately Small Channels, *Adv. Membr.*, 2022, **2**, 1–12, DOI: **10.1016/j.advmem.2022.100043**.

207 W. Song and M. Kumar, Artificial Water Channels: Toward and beyond Desalination, *Curr. Opin. Chem. Eng.*, 2019, **25**, 9–17, DOI: **10.1016/j.coche.2019.06.007**.

208 M. Barboiu, Artificial Water Channels, *Angew. Chem., Int. Ed.*, 2012, **51**, 11674–11676, DOI: **10.1002/anie.201205819**.

209 J. Köfinger, G. Hummer and C. Dellago, Single-File Water in Nanopores, *Phys. Chem. Chem. Phys.*, 2011, **13**, 15403–15417, DOI: **10.1039/c1cp21086f**.

210 J. Köfinger, G. Hummer and C. Dellago, Macroscopically Ordered Water in Nanopores, *Proc. Natl. Acad. Sci. U. S. A*, 2008, **105**, 13218–13222, DOI: **10.1073/pnas.0801448105**.

211 D. J. Mann and M. D. Halls, Water Alignment and Proton Conduction inside Carbon Nanotubes, *Phys. Rev. Lett.*, 2003, **90**(1–4), 195503, DOI: **10.1103/PhysRevLett.90.195503**.

212 M. Majumdar, N. Chopra, R. Andrews and B. J. Hinds, Enhanced Flow in Carbon Nanotubes, *Nature*, 2005, **483**, 44, DOI: **10.1038/438044a**.

213 P. M. Budd, N. B. McKeown and D. Fritsch, Polymers of Intrinsic Microporosity (PIMs): High Free Volume Polymers for Membrane Applications, *Macromol. Symp.*, 2006, **245–246**, 403–405, DOI: **10.1002/masy.200651356**.

214 Y. Ye, L. Gong, S. Xiang, Z. Zhang and B. Chen, Metal–Organic Frameworks as a Versatile Platform for Proton Conductors, *Adv. Mater.*, 2020, **32**, 1–28, DOI: **10.1002/adma.201907090**.

215 K. Geng, T. He, R. Liu, S. Dalapati, K. T. Tan, Z. Li, S. Tao, Y. Gong, Q. Jiang and D. Jiang, Covalent Organic Frameworks: Design, Synthesis, and Functions, *Chem. Rev.*, 2020, **120**, 8814–8933, DOI: **10.1021/acs.chemrev.9b00550**.

216 E. Licsandru, I. Kocsis, Y. X. Shen, S. Murail, Y. M. Legrand, A. Van Der Lee, D. Tsai, M. Baaden, M. Kumar and M. Barboiu, Salt-Excluding Artificial Water Channels Exhibiting Enhanced Dipolar Water and Proton Translocation, *J. Am. Chem. Soc.*, 2016, **138**, 5403–5409, DOI: **10.1021/jacs.6b01811**.

217 M. Barboiu, Y. Le Duc, A. Gilles, P. A. Cazade, M. Michau, Y. Marie Legrand, A. Van Der Lee, B. Coasne, P. Parvizi, J. Post and T. Fyles, An Artificial Primitive Mimic of the Gramicidin-A Channel, *Nat. Commun.*, 2014, **5**, 2–9, DOI: **10.1038/ncomms5142**.

218 C. J. Porter, J. R. Werber, M. Zhong, C. J. Wilson and M. Elimelech, Pathways and Challenges for Biomimetic Desalination Membranes with Sub-Nanometer Channels, *ACS Nano*, 2020, **14**, 10894–10916, DOI: **10.1021/acsnano.0c05753**.

219 P. Chaturvedi, N. K. Moehring, P. Cheng, I. Vlassiouk, M. S. H. Boutilier and P. R. Kidambi, Deconstructing Proton Transport through Atomically Thin Monolayer CVD Graphene Membranes, *J. Mater. Chem. A*, 2022, **10**, 19797–19810, DOI: **10.1039/d2ta01737g**.

220 L. Ruiz, Y. Wu and S. Keten, Tailoring the Water Structure and Transport in Nanotubes with Tunable Interiors, *Nanoscale*, 2015, **7**, 121–132, DOI: **10.1039/c4nr05407e**.

221 R. H. Tunuguntla, Y. Zhang, R. Y. Henley, Y. C. Yao, T. A. Pham, M. Wanunu and A. Noy, Enhanced Water Permeability and Tunable Ion Selectivity in Subnanometer Carbon Nanotube Porins, *Science*, 2017, **359**, 792–796, DOI: **10.1126/science.aan2438**.

222 Z. Shang, R. Wycisk and P. Pintauro, Electrospun Composite Proton-Exchange and Anion-Exchange Membranes for Fuel Cells, *Energies*, 2021, **14**, 1–21, DOI: **10.3390/en14206709**.

223 M. A. Markowitz, V. Janout, D. G. Castner and S. L. Regen, Perforated Monolayers: Design and Synthesis of Porous and Cohesive Monolayers from Mercurated Calix[*n*]Arenes, *J. Am. Chem. Soc.*, 1989, **111**, 8192–8200, DOI: **10.1021/ja00203a020**.

224 G. Yu and X. Chen, Host–Guest Chemistry in Supramolecular Theranostics, *Theranostics*, 2019, **9**, 3041–3074, DOI: **10.7150/thno.31653**.

225 C. J. Addonizio, B. D. Gates and M. J. Webber, Supramolecular "Click Chemistry" for Targeting in the Body, *Bioconjugate Chem.*, 2021, **32**, 1935–1946, DOI: **10.1021/acs.bioconjchem.1c00326**.

226 Z. Zhang, X. Sui, P. Li, G. Xie, X. Y. Kong, K. Xiao, L. Gao, L. Wen and L. Jiang, Ultrathin and Ion-Selective Janus Membranes for High-Performance Osmotic Energy Conversion, *J. Am. Chem. Soc.*, 2017, **139**, 8905–8914, DOI: **10.1021/jacs.7b02794**.

227 Y. Liang, Y. Zhu, C. Liu, K. R. Lee, W. S. Hung, Z. Wang, Y. Li, M. Elimelech, J. Jin and S. Lin, Polyamide Nanofiltration Membrane with Highly Uniform Sub-Nanometre Pores for Sub-1 Å Precision Separation, *Nat. Commun.*, 2020, **11**, 1–9, DOI: **10.1038/s41467-020-15771-2**.

228 M. Elimelech and W. A. Phillip, The Future of Seawater and the Environment, *Science*, 2011, **333**, 712–717, DOI: **10.1126/science.1200488**.

229 S. Faucher, N. Aluru, M. Z. Bazant, D. Blankschtein, A. H. Brozena, J. Cumings, J. Pedro De Souza, M. Elimelech, R. Epsztein, J. T. Fourkas, A. G. Rajan, H. J. Kulik, A. Levy, A. Majumdar, C. Martin, M. McEldrew, R. P. Misra, A. Noy, T. A. Pham, M. Reed, E. Schwegler, Z. Siwy, Y. Wang and M. Strano, Critical Knowledge Gaps in Mass Transport through Single-Digit Nanopores: A Review and Perspective, *J. Phys. Chem. C*, 2019, **123**, 21309–21326, DOI: **10.1021/acs.jpcc.9b02178**.

230 W. Choi, Z. W. Ulissi, S. F. E. Shimizu, D. O. Bellisario, M. D. Ellison and M. S. Strano, Diameter-Dependent Ion Transport through the Interior of Isolated Single-Walled Carbon Nanotubes, *Nat. Commun.*, 2013, **4**, 1–8, DOI: **10.1038/ncomms3397**.

231 X. Liang, Y. Tian, Y. Yuan and Y. Kim, Ionic Covalent Organic Frameworks for Energy Devices, *Adv. Mater.*, 2021, **2105647**, 1–31, DOI: **10.1002/adma.202105647**.

232 Y. Yan, Z. Liu, T. Wan, W. Li, Z. Qiu, C. Chi, C. Huangfu, G. Wang, B. Qi, Y. Yan, T. Wei and Z. Fan, Bioinspired Design of Na-Ion Conduction Channels in Covalent Organic Frameworks for Quasi-Solid-State Sodium Batteries, *Nat. Commun.*, 2023, **14**, 1–14, DOI: **10.1038/s41467-023-38822-w**.

233 C. Wang, Y. Tian, W. Chen, X. Lin, J. Zou, D. Fu, X. Yu, R. Qiu, J. Qiu and S. Zeng, Recent Progress in Covalent Organic Frameworks for Cathode Materials, *Polymers*, 2024, **16**, 5–8, DOI: **10.3390/polym16050687**.

234 S. Mukhopadhyay, A. Das, T. Jana and S. K. Das, Fabricating a MOF Material with Polybenzimidazole into an Efficient Proton Exchange Membrane, *ACS Appl. Energy Mater.*, 2020, **3**, 7964–7977, DOI: **10.1021/acsaem.0c01322**.

235 S. K. Dishari Ionomers with Macrocyclic Calix[n]Arene Moieties for Ion Conductivity and Permselectivity (Patent), 17/996, 666, 2021.

236 C. Crivello, S. Sevim, O. Graniel, C. Franco, S. Pane, J. Puigmarti-Luis and D. Munoz-Rojas, Advanced Technologies for the Fabrication of MOF Thin Films, *Mater. Horiz.*, 2021, **8**, 168–178, DOI: **10.1039/d0mh00898b**.

237 Y. Nagao, Proton-Conductivity Enhancement in Polymer Thin Films, *Langmuir*, 2017, **33**, 12547–12558, DOI: **10.1021/acs.langmuir.7b01484**.

238 T. A. Zawodzinski, T. E. Springer, J. Davey, R. Jestel, C. Lopez, J. Valeria and S. Gottesfeld, A Comparative Study of Water Uptake By and Transport Through Ionomeric Fuel Cell Membranes, *J. Electrochem. Soc.*, 1993, **140**, 1981–1985, DOI: **10.1149/1.2220749**.

239 M. Holz, S. R. Heil and A. Sacco, Temperature-Dependent Self-Diffusion Coefficients of Water and Six Selected Molecular Liquids for Calibration in Accurate 1H NMR PFG Measurements, *Phys. Chem. Chem. Phys.*, 2000, **2**, 4740–4742, DOI: **10.1039/b005319h**.

240 N. J. English and J. M. D. MacElroy, Hydrogen Bonding and Molecular Mobility in Liquid Water in External Electromagnetic Fields, *J. Chem. Phys.*, 2003, **119**, 11806–11813, DOI: **10.1063/1.1624363**.

241 A. Horner, F. Zocher, J. Preiner, N. Ollinger, C. Siligan, S. A. Akimov and P. Pohl, The Mobility of Single-File Water Molecules Is Governed by the Number of H-Bonds They May Form with Channel-Lining Residues, *Sci. Adv.*, 2015, **1**, 1–6, DOI: **10.1126/sciadv.1400083**.

242 E. Zamani, T. J. Johnson, S. Chatterjee, C. Immethun, A. Sarella, R. Saha and S. K. Dishari, Cationic Π-Conjugated Polyelectrolyte Shows Antimicrobial Activity by Causing Lipid Loss and Lowering Elastic Modulus of Bacteria, *ACS Appl. Mater. Interfaces*, 2020, **12**, 49346–49361, DOI: **10.1021/acsami.0c12038**.

243 E. Zamani, S. Chatterjee, T. Changa, C. Immethun, A. Sarella, R. Saha and S. K. Dishari, Mechanistic Understanding of the Interactions of Cationic Conjugated Oligo- and Polyelectrolytes with Wild-Type and Ampicillin-Resistant Escherichia Coli, *Sci. Rep.*, 2019, **9**, 1–12, DOI: **10.1038/s41598-019-56946-2**.